

Reply to Reviewers' comments

We are grateful to the Editor and the Reviewers for their precious times in reviewing our manuscript. These valuable comments are very helpful for the improvement of the quality and clarity of the manuscript. We have addressed all comments as detailed below and in the updated manuscript. All the changes in the revised manuscript are shown in blue. If further responses should be made, please let us know, and thanks a lot for your consideration.

Editor:

1. As one reviewer indicated, "English needs to be improved; Chinese style English can be seen in many places throughout the manuscript". I urge you to have a native English speaker or a person with good English writing to read through your manuscript carefully to improve the manuscript writing. I can see many grammar errors. This is especially important for your paper to improve its readability in order to gain a wider attention in the international community, and to meet the high standard of ACP.

Response: Thank you very much for your valuable comments. We have gone throughout the entire manuscript, sentence by sentence, with the help of a native speaker and revised the manuscript carefully.

2. You need to define the East Asia domain in the first place when using it.

Response: Thank you for your nice reminder. The definition was clarified in the revised Fig. 1 caption.

3. Table 2 caption, is it "clean" episodes?

Response: Thank you very much for your reminder. We have corrected in the revised manuscript.

4. Abstract is too long, and try to condense it.

Response: Thank you for the important comment, the valuable suggestions have been taken into account.

Referee #3:

1. Fig. 2, why do not also look at precipitation? It is highly related to the aerosol wet removal, and hence the aerosol loading and AOD. When checking precipitation, a few days before the events may also be important, because it will affect the accumulation of pollutants. If there is no precipitation in any investigated days, please clarify in the paper.

Response: Thank you very much for your important reminder. The reasons why we do not look at precipitation are illustrated as follows:

- 1) As you pointed out, precipitation is an important mechanism of aerosol removal. Therefore, as indicated in the Introduction, we choose the autumn to study to minimize the effect of wet deposition since autumn is the season with less precipitation in East China.
- 2) The atmosphere structure of autumn is more stable and mainly influenced by large-scale synoptic systems; the dynamic impact is stronger than the thermal effect. These factors reduce the influences of complex mesoscale and small-scale weather systems and the thermal effect on precipitation. Thus, the precipitation tends to be caused by certain large-scale atmospheric circulations.
- 3) In addition, except one clean episode identified as the passage of cold front (10/23-10/26 in 2008), which is accompanied by significant precipitation, there is no occurrence of large scale precipitation during any other selected episodes (including the day before the episode and the corresponding consecutive days). The regional mean value of clean episodes that with precipitation is only about 1mm/day, which is equivalent to that of pollution episodes.
- 4) The aforementioned reasons indicated that the precipitation in autumn is closely related to the large scale circulations and it does not influence the conclusions from our study. In addition, in this study, we put emphasis on the impacts of atmospheric circulations, consequently, did not show the discussion of precipitation separately in Fig. 2.

The relevant interpretations have been added to the revised manuscript, Thanks again!

2. Please clarify in the caption about what are the meanings of T1-T9 in Fig. 18.

Response: Many thanks for your careful reminder. T1-T9, namely Type 1-Type 9, mean nine different types summarized in this study. We have clarified in the revised manuscript

3. In Fig. 8-16, it seems that temperature is also higher in the polluted cases than that in the clean cases, particularly for type 1 and 2. Please discuss some potential impact of the higher temperature on the increase of pollutants.

Response: Thank you very much for your valuable comment. Based on your suggestion, we check the temperature of nine types carefully, and the regional mean value of AOD and temperature are presented.

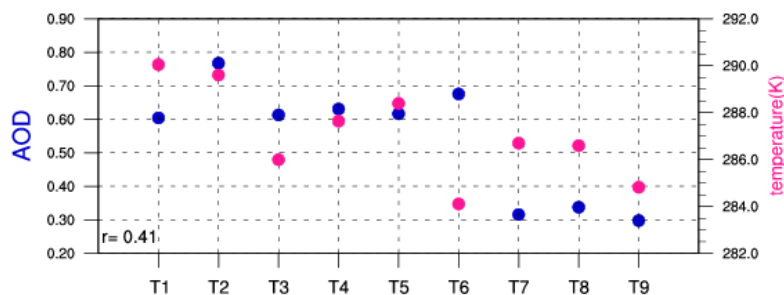


Fig. A. The regional mean value of AOD and surface temperature in East China for nine types.

On one hand, the surface temperature of T1 and T2 are indeed higher as shown in Fig. A. However, the temperature of T3 is significantly lower than T1 although both are pollution types (with similar AOD). And the temperature of T3, T7 and T8 are nearly equal to each other, their corresponding AOD values are different. The mean AOD of types 7 and 8 are merely half of Type 3. Besides, the temperature of T6 is the lowest among nine types, although its AOD is second only to T2. Furthermore, the correlation coefficient between AOD and surface temperature is 0.41, which does not pass over 90% confidence level. So these two variables do not show a clear relationship in our study. On the other hand, T1 is characterized as the pattern before the passage of the cold front. Before the arrival of cold flow, warm air mass accumulates ahead of the front and may cause higher temperature. Moreover, most pollution types are under the control of high pressure (anticyclonic circulation) and the fine weather is always accompanied by higher temperature. Meanwhile, more than 80% clean episodes are influenced by strong cold air flow from northwest, which may lead to lower surface temperature, such as T9 identified as the passage of cold front. Therefore, the large-scale temperature is closely associated with the atmospheric circulations.

Concerning that quite a few studies focused on the impacts of temperature on AOD, the detailed relationship between the two variables needs more investigations and additional datasets. We would like to analyze the impacts of local temperature on the distribution of aerosols in similar large-scale atmospheric circulation patterns in the future work! We have discussed the issue in section 3.4 of the revised manuscript.

4. Yang et al., 2013 is not in the reference list.

Response: Thank you for your nice reminder. We have added the reference in the

revised manuscript.

Yang, Y. J., Fu, Y. F., Wu, B. W., Shi, C. E., Deng, X. L., Zhang, H., Zhang, Y.: Impacts of Agricultural Fire on Aerosol Distribution over East China during Summer Harvest time, *Journal of Atmospheric and Environmental Optics*, 8(4): 241-252, 2013. (in Chinese)

Impacts of Atmospheric Circulations on Aerosol Distributions in Autumn over East China: Observational Evidences

Xiaoyi Zheng¹ Yunfei Fu^{1,2,3} Yuanjian Yang^{1,3} Guosheng Liu^{1,4}

1. School of Earth and Space Sciences, University of Science and Technology of China, Hefei, 230026, PR China;

2. State Key Laboratory of Severe Weather, Chinese Academy of Meteorological Sciences, Beijing, 100081, PR China;

3. Key Laboratory of Atmospheric Sciences and Satellite Remote Sensing of Anhui Province, Anhui Institute of Meteorological Sciences, Hefei, 230031, PR China;

4. Department of Meteorology, Florida State University, Tallahassee, FL 32306-4520, USA

Corresponding author address:

Yunfei Fu

School of Earth and Space Sciences, University of Science and Technology of China,
Hefei, 230026, PR China

Phone: 86-551-63606897; Fax: 86-551-63606897

E-mail: fyf@ustc.edu.cn

Submitted to *Atmospheric Chemistry and Physics*

ABSTRACT

Regional heavy pollution events in East China (110°E-122°E, 28°N-40°N) are causing serious environmental problems. In this study, the relationship between the degree of regional pollution and the patterns of large scale atmospheric circulation over East China in October is investigated using ten-year (2001-2010) Terra/MODIS aerosol optical depth and NCEP reanalysis data by both case study and composite analysis. Eighteen polluted and ten clean episodes are selected and categorized into six polluted types and three clean types, respectively. Generally speaking, weather patterns such as a uniform surface pressure field in East China or a steady straight westerly in middle troposphere, particularly when being at the rear of anticyclone at 850hPa, are typically responsible for heavy pollution events. Meanwhile, clean episodes occur when strong southeastward cold air advection prevails below the middle troposphere or air masses are transported from sea to land. Uniform descending motion prevails over the study region, trapping pollutants in the lower atmosphere. Therefore, the value of vertical velocity averaged from 1000hPa to 100hPa and divergence of wind field in lower troposphere are used in this study to quantify the diffusion conditions in each circulation type. The results reveal that it is often a clean episode when both the mean downward motion and the divergence of low level winds are strong (large than $2.56 \times 10^{-2} \text{ Pas}^{-1}$ and $1.79 \times 10^{-2} \text{ s}^{-1}$ respectively). Otherwise, it is more likely to be a pollution episode.

Key words: East China, AOD, atmospheric circulations, pollution episodes, clean episodes

1. Introduction

Since aerosols can modulate the radiation budget of the earth-atmosphere system, influence the climate, and degrade air quality (Kaufman et al. 2002), they have long been attracted high attentions from scientific community (Twomey 1977; Rosenfeld et al. 2004; Zhao et al. 2006a, 2006b; Rosenfeld et al. 2007; Li et al. 2011; Koren et al. 2012; Zhao et al. 2012; Zhao et al. 2013a, 2013b; Chen et al. 2014). Particularly, with the rapid urban growth and development of various industries during last decades, the high concentration of atmospheric pollutants has become one of the major environmental problems, which usually pose threats to human health (Donaldson et al. 2001; Kan and Chen 2004; Janssen et al. 2011). To understand the mechanisms that control spatiotemporal distribution of aerosols, extensive investigations have been carried out to study the relationship between the air quality and multiple factors. Among the multifaceted problems related to air pollution, favorable weather condition is a factor that should not be ignored (Zhao, et al., 2010; Xu et al., 2011). In general, although the characteristics of regional air quality depend on many complex elements, the major contributors are the emission of the pollutants compared with favorable large scale meteorological conditions (Chen et al. 2008a; Chen et al. 2008b). Ziomas et al. (1995) pointed out that in an urban environment, the serious air pollution episodes are not attributed to sudden increases in the emission of pollutants, but caused by meteorological conditions that are unfavorable for dispersion. Normally, the anthropogenic emissions of widespread pollutant sources are quasi-stable in East China, the degree of air pollution in the region is largely subject to large scale atmospheric

conditions (Xu et al. 2011). In some other regions, strong links between the concentration of aerosols and certain synoptic weather condition have already been identified (Demuzere et al. 2009; Saavedra et al. 2012). It has also been revealed that under the circumstances of the same pollutant emission quantity, the ground concentration of pollutants **varies** directly with different synoptic patterns (Wang et al. 2001).

Weather conditions **as represented by** a number of meteorological parameters, such as wind speed and direction, temperature, relative humidity, precipitation etc., and synoptic patterns **as** analyzed in terms of atmospheric circulations, can contribute to the vertical redistribution and long-range transport of air pollutants, **which leads to either accumulation or dispersion of aerosols** (Cheng et al. 2007; Ding et al. 2009). A growing body of research is showing the important effects of weather conditions on **determining the** distribution of pollutants and atmospheric pollution levels. For example, Tanner and Law (2002) investigated the impacts of meteorological parameters (wind speed, wind direction, temperature, relative humidity and solar radiation intensity) on the frequency of high-level pollution episodes in Hong Kong. Ding et al. (2004) successfully simulated the wind patterns of sea-land breezes and the planetary boundary layer (PBL) heights to illustrate the meteorological cause of the photochemical ozone episode associated with Typhoon Nari in the Pearl River Delta of China. They **compared** the characteristics of dispersion and transport **during** pre-episode and episode days. Xu et al. (2011) confirmed the deterministic impacts of wind speed and wind direction on the concentration of various trace gases at a suburban site between 2 mega-cities. Csavina

et al. (2014) examined dust events in two semi-arid sites, and then showed a complex, nonlinear dependence of PM₁₀ on wind speed and relative humidity.

The synoptic scale circulations represent a certain atmospheric condition at a given region through its close association with various meteorological parameters such as wind speed, wind direction, temperature, etc. (Shahgedanova et al., 1998; Kassomenos et al., 2003; Chen et al., 2009). Consequently, instead of using individual meteorological parameters, several studies have been carried out based on atmospheric circulation patterns. For example, Shahgedanova (1998) employed principal component analysis and cluster analysis for Moscow to develop seasonal synoptic indices to examine weather-induced variability in CO and NO₂ concentrations, and concluded that anticyclonic conditions in spring, summer and autumn are introductive to high pollution levels. Flocas et al. (2008) assessed the circulation patterns at the mean sea level for a period of 15 years and distinguished four synoptic scale types. They found the presence of an anticyclone accounted for the highest percentage of pollution episode over Greece. Moreover, Zhang et al. (2010) used a numerical model to simulate the impact of weak/strong monsoon circulations on interannual variations of aerosols over eastern China under the conditions of the same anthropogenic emissions, and suggested that the decadal-scale weakening of the East Asian summer monsoon is responsible for the increase in aerosol concentrations over eastern China. Using satellite products, Zhao et al. (2010) showed consistent disappearance of CO and O₃ enhancements over southeastern China at the onset of East Asian summer monsoon and the reemergence after the monsoon wanes, which confirmed the strong modulation of monsoon system

on regional air quality. Liu et al. (2013) further demonstrated a potential influence from the variation of large-scale circulation, El Nino Southern Oscillation, upon the interannual fluctuation of summertime aerosol optical depth (AOD). Russo et al. (2014) applied the analysis on 10 basic circulation weather types characterized by a set of indices, and their results showed that easterlies prevailed during pollution episodes of three pollutants (NO₂, PM₁₀, O₃) in Portugal.

The aforementioned works suggest that synoptic types play a crucial role in the formation of a pollution episode. They established a predictive connection between air quality and circulation patterns over various regions, and provided valuable scientific basis for weather forecast operations. To the authors' knowledge, even though some attempts have been conducted to study the similar relationships in China, most of them chose to study the connection over a single city (Wang et al 2007, Chen et al. 2008b, Guo et al 2013) rather than over a regional scale (e.g., East China in this study). East China, as a highly urbanized region, with rapidly increasing of industrial and automotive emissions, is frequently characterized by poor air quality (Ding et al., 2008; He et al. 2012). Therefore, establishing a predictable relationship between circulation pattern and air quality is important for early prediction of pollution episodes.

In the present study, we evaluate the above relationship during autumn using ten-year (2001-2010) Terra/MODIS (Moderate-resolution Imaging Spectroradiometer) AOD product and atmospheric circulations derived from NCEP (National Centers for Environmental Prediction) reanalysis data. The choice of autumn is in consideration of the following reasons. First, the wet deposition effect is weaker due to less precipitation

in autumn (Chen et al. 2012), which also ensures the availability of AOD data. Second, in contrast with other seasons, the local atmosphere structure of autumn is stable and mainly influenced by large-scale synoptic systems; the dynamic impact is stronger than the thermal effect. These factors reduce the influences of complex mesoscale and small-scale weather systems and the thermal effect on precipitation. Therefore, precipitation in this season tends to be caused by certain large-scale atmospheric circulations, which makes it more suitable for the study of impacts from large-scale atmospheric circulations. Finally, previous researches rarely focused on the pollution episodes during autumn. In addition, Anhui province is taken as an example to show the pollution level of each month in East China (Yang et al., 2013). The occurring frequency of haze days for Anhui is the highest in October during a whole year based on the measurements from 80 meteorological observation stations. Therefore, October is selected as a representative autumn month for our present work. The rest of the paper is organized as follows. A brief description of the data and processing methodology used in this study is presented in Section 2. In Sections 3 and 4, we describe the interannual variability of AOD over East China and then explore the relationships between AOD and characteristics of synoptic circulations through statistical and synthetic analysis. Conclusions are given in Section 5, in which the association of various circulation types with different AOD spatial distributions over East China is summarized.

2. Data and Methods

Data used in this study and methods for selecting high/low AOD cases are described in this section. The research considers the time period from 2001 to 2010

over the region of 28°N to 40°N and 110°E to 122°E.

2.1 Pollution data

The main data set used to describe air quality is the daily averaged Collection 5.1 level 3 AOD products (at 1 ° horizontal resolution) derived from the [Terra's MODIS measurements](#) (accessible from <http://ladsweb.nascom.nasa.gov/data/search.html>).

Unlike ground based data, MODIS provides long-term continuous observations for the spatial and temporal distribution of aerosol, suitable for the investigation of this study.

AOD measures the degree to which aerosols prevent the transmission of light by scattering and absorption. By using the Terra/MODIS aerosol data, Kim et al. (2007) evaluated the temporal and spatial variation of aerosols over East Asia. Wu et al. (2013) pointed out that MODIS data were usually valid throughout China and revealed the characteristics of aerosol transport and different extinction features in East Asia. Luo et al. (2013) verified the good quality of MODIS AOD over land in China and used 10 years data to construct the climatology of AOD over China. Based on the previous validations, MODIS AOD data are considered to have good quality over China region and can capture the features of aerosol distribution.

In fact, the AOD data have been widely used to enhance the understanding of changes in air quality over local, regional, and global scales as a result of their sensitivity to total abundance of aerosols (Chu et al. 2002; Al-Saadi et al. 2005; Lin et al. 2010). AOD can indicate the air quality to a certain degree; the higher the AOD value is, the worse air quality becomes (Liu et al. 2013). In this study, we discuss the cases of pollution and clean separately.

Finally, the Collection 5 MODIS active fire product (MCD14ML) is used to monitor the influences of the sudden enhanced emissions from biomass burning. The monthly fire location product contains the geographic location, date, and some additional information for each fire pixel on a monthly basis. In this study, only those Terra-observed pixels with fire detection confidence greater than 60% are used.

2.2 Meteorological Data

The corresponding atmospheric field analyses performed in this paper are based on the results of meteorological reanalysis products made available by NCEP and National Center for Atmospheric Research (NCAR). For a complete discussion, we consider both surface and upper-air circulation patterns. The sea level pressure (SLP) field, which is closely related to the meteorological factors, is selected to characterize a certain synoptic episode. The 850hPa and 500hPa levels are selected as the typical height of lower and middle troposphere, respectively. Mean sea level pressure, temperatures at surface and the 500hPa level, geopotential heights at the 850hPa and 500hPa level, as well as relative humidity, wind field and vertical velocity were extracted from NCEP/NCAR Reanalysis dataset on a $2.5^\circ \times 2.5^\circ$ latitude/longitude grid on a daily basis (<http://www.esrl.noaa.gov/psd/data/gridded/data.ncep.reanalysis.html>).

2.3 Methods

On the basis of ten-year October data, namely 310 days, we get the daily AOD distribution. According to the threshold of AOD (mentioned in section 3.1), the whole

310 days are divided into four categories: high AOD (>0.6), low AOD (<0.4), moderate AOD (0.4~0.6) and the missing-value day (due to clouds). Ignoring the group of missing and moderate AOD data, the circulation fields correspond to the other two categories (high AOD and low AOD) are evaluated at the same time. Since satellite-based AOD exists certain uncertainties, the consecutive days of high (or low) value can better illustrate the existence of the air pollution than just one day. And statistical results of two categories also show that the occurrence of high (or low) value of AOD tends to last for several days. Additionally, the corresponding circulation pattern is also quasi-steady during these high (or low) AOD periods.

Taking the above facts into account, the first synthetic process is conducted by averaging the corresponding grid point values for a number of successive days (greater than or equal to 2 days) to represent high (or low) AOD conditions. Following this approach, 28 episodes, among which there are 18 high-value episodes (HEs) and 10 low-value episodes (LEs), are initially identified during 2001-2010. In order to obtain the statistical characteristics of the pollution and clean episodes, the second synthetic process is performed. We classify the 18 HEs and 10 LEs obtained in the first step on a synoptic basis and average the similar circulations for these two different categories respectively, a thorough description of results obtained by this method can be found in section 3.3. The 18 HEs are clustered into six types while the 10 LEs are three types. Thus, nine distinct circulation types are consequently considered in the following analyses.

2.4 Hybrid Single-Particle Lagrangian Integrated Trajectory (HYSPLIT) Model

The backward trajectories for two typical episodes discussed in section 3.2 are simulated using the HYSPLIT model, employing NCEP/NCAR reanalysis meteorological data as input fields. With powerful computational capabilities, the HYSPLIT_4 model is a widely-used system for calculating simple trajectories to complex dispersion and deposition simulations using either puff or particle approach (readers are referred to Draxler and Hess (1997) for [details](#) of the model). Borge et al. (2007) used back trajectories computed with HYSPLIT model to examine the impact of long-range atmospheric transport on urban PM₁₀ for three cities. Chen et al. (2013) incorporated eight size PM fractions of metals to the HYSPLIT model and provided a prediction of the size distribution and concentrations of heavy metals. In this work, the air-mass trajectories are evaluated in order to present the different movement of air parcels during the two [opposite](#) episodes.

3. Results

3.1 Climatological mean and interannual variation

Prior to the analysis of the link between air quality and large-scale circulations, it is necessary to reveal the climatological mean and interannual variation of AOD in October over East China. The climatological mean AOD from MODIS are obtained for the period from 2001 to 2010. As shown in Figure 1a, the spatial distribution shows [that](#) AOD ranges from 0.3 to 0.9 for almost the entire area. Four prominent centers of high AOD values are found in East China, i.e., Bohai Gulf, Yangtze River delta, junctional areas of Anhui, Shangdong and Henan provinces, and most parts of Hubei and Hunan provinces [where it](#) were recognized as the source of high emissions in

October according to Wang and Zhang (2008). In other words, these centers are considered as possible consequences of industrial emissions or agricultural biomass burning that occurs in autumn under certain meteorological conditions. Figure 1b presents the standard deviation of AOD for the same period. The distribution pattern of Figure 1b is similar to that of Figure 1a, which means that the standard deviation is also larger over the regions where the mean AOD is higher. Moreover, as shown by the climatological means of wind vectors at 850hPa and geopotential height in Figures 1c and 1d, weak clockwise winds at 850hPa (Figure 1c) and flat western flow at 500hPa (Figure 1d) suggest that East China is dominated by the large-scale stable circulation without the frequent disturbances of small-scale weather systems for October. As for vertical structure, Figures 1e and 1f present height-latitude cross-sections of vertical velocity and divergence of wind, respectively. In Figure 1e, the positive value indicates uniform descending motion over the East China. Figure 1f also shows convergence in upper and divergence in lower altitudes, which are favorable to the maintenance of downward atmospheric motion. Interannually, we show the ten-year distribution of AOD over East China in October (spatial distribution in Figure 2a and regional mean in Figure 2b).

As indicated by Ziomas et al. (1995) and Xu et al. (2011), in a given season, the anthropogenic emissions are almost constant, while the biomass burning in rural areas may cause a sudden increase in pollution emissions. Consequently, we combine MODIS fire product with NCEP relative humidity, which could influence AOD via light extinction efficiency of aerosols, and wind speed, which may modulate the

concentration of aerosols, to explore the annual variations. As shown in Figure 2b, the interannual variation of fire number in the East China is weakly correlated with that of AOD. For example, the AOD of 2003 is lower than 2006, but fire number is larger. It implies that there are other factors contributed to the variation of AOD. For the relative humidity, it is around 55% for all years except 2001 and 2009. Namely, the variation of the relative humidity is not clear. Furthermore, as demonstrated by Twohy et al. (2009), the elevated relative humidity can cause an increase of AOD owing to its impacts on hydrophilic aerosols. However, in our data the correlation coefficient between relative humidity and AOD is -0.4, which did not pass the 90% confidence level. On the other hand, the correlation between wind speed and AOD is significant (-0.63) at 95% confidence level, which indicates that the decrease of AOD value occurs with the increase of wind speed. Based on the above results, it is deduced that the interannual variation of AOD in East China, to a certain extent, is determined by the vertical and horizontal movements of air flows, which can influence the spatio-temporal distribution of aerosols.

In order to depict the frequency of pollution event and give the threshold beyond which the value can be regarded as high AOD, we examine the frequency distribution of high AOD (>0.5 and >0.6) as plotted in Figure 3. Luo et al. (2014) considered the value of AOD>0.5 as the high value in China. However, in our data for more than half of East China, the frequency of AOD>0.5 is larger than 50% (Figure 3a). Consequently, we define a more rigorous critical value, 0.6, as the high AOD threshold. Compared to Figure 3a, the area with relative high frequency of high AOD with the new threshold

reduces in Figure 3b; the high AOD frequency of above 65% area of East China is less than 50%. On the other hand, a day is classified into the low-value group if the value of regional mean AOD over the study area is less than 0.4. Xin et al (2014) investigated the relationships between daily observed PM_{2.5} concentration and AOD in North China, and pointed out that there was a high correlation between the two variables in autumn with a correlation coefficient (R^2) being 0.57. Therefore, the MODIS AOD is valuable and capable in retrieving the surface PM_{2.5} concentration. Using the linear regression functions derived by Xin et al. (2014), when AOD is 0.4 (0.6), the PM_{2.5} concentration is calculated to be 72.34 $\mu\text{g m}^{-3}$ (104.62 $\mu\text{g m}^{-3}$). These two values correspond to moderate and lightly polluted in China, respectively, supporting our definition of AOD thresholds being suitable. Furthermore, according to the topography shown in Figure 3c, it is evident that the emergence of high frequency is related closely to the terrain of East China. It is noted that the pattern of high frequency distribution in Figure 3b is consistent with that of high values of ten-year mean AOD distribution in Figure 1a. High AOD mainly concentrated in plains and hilly areas, especially the economically developed Yangtze River Delta, where it is characterized by dense population along with a great number of industrial and motor vehicle emissions.

Since MODIS-AOD represents for the aerosol column abundance rather than the content of pollutants near the surface, the upward motion alone (which favors the diffusion of pollution) cannot change the value of AOD. Moreover, the aforementioned two vertical cross-sections illustrate that the climatological mean vertical velocity averaged from 1000hPa to 100hPa in autumn over East China is downward of 2.56×10^{-2}

2 Pas^{-1} . This suggests that the strong downdraft leads to a more concentrated vertical distribution of pollutants, which gathers pollutants together in the lower layer. As a result, AOD will mainly depend on the divergence of low level wind field in autumn over East China. Strong divergence of wind field in the lower troposphere facilitates the diffusion of aerosols, whereas weak divergence favors the formation of poor air quality. As shown in Figure 1f, the climatological mean divergence, averaged from 1000hPa to 850hPa, of lower troposphere is $1.79 \times 10^{-6} \text{ s}^{-1}$.

The relationships among the AOD, vertical velocity and divergence during the study period are shown in Figure 4a. According to the climatological mean of vertical velocity and the low level divergence, we divide the samples into four categories: C1, C2, C3, and C4. There are significant differences in vertical velocity and divergence between the distribution of high AOD group and low AOD group. For example, the group with AOD less than 0.4 mainly distributed in C1, in which both the vertical velocity and divergence are relative strong. The increasing values of AOD occur with the decreasing values of vertical velocity and divergence of low level winds. The bottom-left corner of the figure is primarily occupied by high AOD group. For a more intuitive representation, Figure 4b shows a histogram of occurrence frequency for high AOD (>0.6) and low AOD (<0.4) group, which correspond to polluted and clean environments, respectively. C1 presents the maximum frequency of low AOD group, which is nearly 60%. Conversely, pollution exists predominantly in the categories with weak divergence, especially in C3, where both of two variables are less than the climatological averages. These results are consistent with our hypothesis and confirm

that the mean vertical velocity and low level divergence of winds resulted from diverse synoptic patterns are indicative of regional air quality.

3.2 Two Typical Cases: High and Low AOD

On the basis of the above results, two typical cases are presented in this section to show the differences between polluted and clean episodes. The event during 28th-31st October 2006 is analyzed as a typical high AOD episode (HE) example, whereas the 4 days from October 21st to 24th in 2003 are selected as a typical low value episode (LE). First of all, we give the fire numbers of two cases, which are 18 for HE and 25 for LE accordingly. Since the difference of sudden enhanced emissions from biomass burning between two cases are little, it can be concluded that AOD difference largely as result of the different atmospheric circulations.

The mean patterns of AOD and atmospheric circulations at surface, 850hPa level, 500hPa level in the period of the HE example are given in Figure 5. The regional averaged AOD of HE was 0.76, and the maximum value was greater than 1.2, which signifies a polluted event. The corresponding sea level pressure pattern (Figure 5b) was almost controlled by uniform pressure field, and the shallow trough promoted west-northwest flow at 500hPa (Figure 5d), all of which represented a stable synoptic pattern and was conducive to the storage of air pollutants. In vertical direction, the clear downward motion is in accordance with climatological pattern of autumn (Figure 5e), and the whole-level averaged value over East China is $3.67 \times 10^{-2} \text{Pas}^{-1}$, leading to an accumulation of aerosols in low layer. During this period, the main feature of wind field at 850hPa level was the weak clockwise circulation centered at Shanxi province; wind

blew from the north in East China under the control of a large scale anticyclone (Figure 5c). The divergence of winds in lower troposphere is $1.62 \times 10^{-6} \text{s}^{-1}$ for HE (Fig. 5f), which is less than the climatological mean and does not favor the outflow of air pollutants.

Figure 6 shows the mean patterns for the LE example from October 21st to 24th in 2003. Unlike the polluted episode (Figure 5a) when the whole East China was masked by high aerosol loading except a small area in northwest, the area was mainly influenced by low AOD (<0.4) (Figure 6a). The mean AOD (0.38) was about half the level that HE case reached. In Figure 6b, the surface circulation of LE in East China was to the front of the high pressure center. The temperature and geopotential height in the middle troposphere (500hPa) indicated a dominant northwesterly flow prevailed over East China and led cold air masses to low-mid latitudes (Figure 6d). Under these conditions, the vertical velocity of LE ($8.05 \times 10^{-2} \text{Pa s}^{-1}$, Figure 6e) is much larger than that of HE over the whole vertical layer, which played an important role in the diffusion of air pollutants when combined with relative strong divergence of winds in low troposphere ($2.86 \times 10^{-6} \text{s}^{-1}$, Figure 6f.), being in contrast to the HE case which showed clear distinctions, specifically the weaker downward atmospheric motion and adverse divergent conditions. Moreover, compared to the northerly of $1-4 \text{ ms}^{-1}$ in HE episode (Figure 5c), stronger northwesterly winds of $6-9 \text{ ms}^{-1}$ were observed at 850hPa (Figure 6c) in LE episode.

In addition, to describe different air mass sources and their transport paths, HYSPLIT model was applied to the days when the two typical episodes occurred. For

each day, we calculated the backward trajectories originated from three locations and the associated ending height is 1000m above ground level. Trajectories were considered to be initiated at 0200 (UTC) when Terra/MODIS passes across China, terminating at the end of 48 hours. As shown in Figure 7, the backward trajectories of four polluted days (Figure 7a) were composed of short tracks, which were mainly trapped in East China. This indicated that the pollution was caused by the combination of the circulation pattern, which acted against dissipation of air pollutants, and a great deal of local emissions in the studied area. In contrast, the LE episode presents a cluster of relatively longer trajectories corresponded to fast-moving air masses from Mongolia. Northwesterly cold winds on these days dispersed local air pollutants, and also brought in clean air.

3.3 All Selected Cases

The aforementioned case studies show that without considering the variations in emission some synoptic types are favorable to the occurrence of the air pollution while others are not. Comprehensive statistics of all cases in the study period over East China is calculated. Excluding all missing and moderate AOD days, a total 120 days are extracted for the research, of which there are 90 days with high AOD and 30 days with low AOD. Table 1 and Table 2 list the statistical results for the 18 pollution episodes and 10 clean episodes, respectively.

It is found from Table 1 that 2002 and 2006 are both years with maximum occurrence (16 days) of pollution, which is consistent with the high value presented in Figure 2. The estimated duration of pollution episodes, on a daily basis, mostly lasts for

about four days or longer. To be more specific, for sea level pressure field, the most frequent pattern is characterized as the periphery of the high pressure centered in the Tibetan plateau or Mongolia, amounts to 38 days. The uniform pressure over the East China is the second high-frequency type with a percentage of 37%, namely 34 days. Among the remaining three types, one is interpreted as the pattern before the passage of a cold front. The corresponding pattern in lower troposphere (850hPa) is characterized as strong cold air flow moving toward the East China, which involves 2 episodes (6 days). The other 15 episodes are dominated by the anticyclonic circulation in 850hPa. It is noted that the region is controlled by the different part of anticyclones. The frequency of the rear of anticyclone is 35 days, while the frequency of the foreside and the center of anticyclone are both 23 days. For the patterns of 500hPa geopotential height, there are 30 days influenced by the northwest (NW) flow, of which 25 days were caused by the upper air trough. The number of days associated with the west-northwest (W-NW) flow and west (W) flow, is 19 and 7, respectively. In addition, the southwest (SW) flow prevailed during a three-day episode.

Table 2 is the same as Table 1, but for 10 clean episodes. Precipitation is an important mechanism of aerosol removal, which may compromise the estimation of effects due to the circulation patterns. In this study, except one episode identified as the passage of cold front (October 23 to 26, 2008), which is accompanied by significant rainfall. There is no occurrence of large scale precipitation during any other episodes, even on the day before the episodes and during consecutive days following the episodes. The regional mean value of clean episodes that with precipitation is only about

1mm/day, which is equivalent to that of pollution episodes. Therefore, it does not influence the results of our study. According to the Table 2, the number of low-value day peak in 2003. The surface high pressure centered in the northwest of China is the frequent pattern, accounting for 15 of the total 30 clean days. Additionally, there are 8 days corresponding to the passage of a cold front, followed by a frequency of 5 days for the rear of a high pressure system over the Yellow Sea. The rest 3 days are characterized by a uniform pressure field. For 850hPa wind fields, the pattern dominated by anticyclonic wind vectors over the study area has the highest frequency of 12 days. The second frequent pattern is the anterior part of anticyclone (10 days), and the rest two episodes are related to the upper air cold front bringing strong and cold airs southwardly in the lower troposphere. The 500hPa geopotential heights of clean episodes, unlike those for polluted episodes, include only two dominant airflow directions. For most of clean days, the northwest flow prevails, whereas the other 5 days are associated with the flat west streams.

The characteristics of circulation patterns of all polluted and clean episodes at each level are gained through the above statistics. In terms of a single level (surface/850hPa/500hPa), the circulation patterns for different episodes are similar to each other. However, it is the combination of circulations at lower level and upper level that the air quality always depends on. The rows in the Table 1 and Table 2 with same capital letters in the parentheses following the sequence number indicate those episodes are affected by the similar circulation patterns in all the three atmospheric levels. There are nine different letters in two tables, namely, the entire 28 episodes are classified into

nine different types, among which there are six polluted types and three clean types.

3.4 Statistics and synthetic analysis

Based on the above results of all cases, nine types are inspected in detail in this section. Before the description of each type, it is pointed out that the mean AOD and meteorological fields for each type, which consist of the sea level pressure, surface temperature, the 850hPa wind and geopotential height, the 500hPa geopotential height and temperature, the vertical velocity and wind divergence, are averaged for the several episodes that are marked with the same letters in Table 1 (Table 2). The percentage of each polluted (clean) type is calculated on a daily basis. More specifically, Figures 8 to 13 present the spatial distribution of mean AOD for six high-value types and the associated large-scale three-dimensional atmospheric circulation structure. Each type contains a set of three different layers, which differ from each other, either in terms of the position and intensity of weather systems or in the vertical allocation of the corresponding atmospheric circulations.

Firstly, the two episodes marked with the letter A in Table 1 are classified as Type 1, which account for 6.7% of all polluted days. Distribution of AOD is shown in Figure 8a; high AOD value appeared in Anhui province and the regional mean AOD is 0.60. The corresponding atmospheric circulations were shown in Figures 8b-8d. In detail, the sea level pressure field is characterized as the pattern before the passage of a cold front. Before the arrival of the cold flow associated with a low-pressure system over northeast of China, warm air mass accumulates ahead of the front, which favors the increase of

pollutants. At higher levels, the area is situated behind the trough, and thus the dominant wind direction in the East is northwest, which gradually leads cold air mixed with northern pollutants toward East China. Even though the vertical downward motion is strong ($5.13 \times 10^{-2} \text{ Pas}^{-1}$), the divergence of winds in lower troposphere is weak ($0.49 \times 10^{-6} \text{ s}^{-1}$). In fact, a convergence of air at 850hPa can be seen in Figure 8c, whereas the wind speed is relative high. In view of the above-mentioned facts, the pollution of this type is not quite serious.

Type 2 (marked with the letter B) is the most frequent among the six polluted types with a percentage of 40%. It is evident that the occurrence of pollution in East China mainly requires a uniform pressure field on surface (Figure 9). At 850hPa level, the pattern corresponds to weak southerlies controlled by the rear sector of an anticyclonic circulation. Additionally, the upper level west-northwest flow is crossing the area. Under those fair weather conditions, both the vertical velocity ($1.97 \times 10^{-2} \text{ Pas}^{-1}$) and divergence ($0.97 \times 10^{-6} \text{ s}^{-1}$ for lower troposphere and $1.08 \times 10^{-6} \text{ s}^{-1}$ for middle level) for Type 2 are less than the climatological mean mentioned earlier, allowing the stagnation of pollutants. According to Table 1, it seems that Type 2 can last for a long time. Generally speaking, Type 2 is a relatively stable and serious pollution example with a mean AOD value of 0.77.

Type 3 (marked with the letter C) is associated with four episodes, accounting for 21.1%. From Figure 10a, high AOD values center in Henan province, extending to the southeast and southwest. The corresponding circulation structure is shown in Figure 10b-10d. Over the surface, the region is governed by the periphery of a high pressure

system located in Mongolia, which results in low pressure gradient over the central of East China. At 500hpa, an upper air trough causes moderate northeasterly flows. The wind field in lower troposphere can be considered as anticyclonic, and the wind direction is consistent with the direction of diffusion of pollutants. From Figure 10e, the strong descending motion dominates, which is $4.91 \times 10^{-2} \text{ Pas}^{-1}$. However, the limited low level speed and divergence of winds ($1.54 \times 10^{-6} \text{ s}^{-1}$), prevent the spread of pollutants to outside the area. These conditions yield a regional averaged AOD value of 0.61.

Type 4 (marked with the letter D) consists of four pollution episodes (accounts for 18.9%), which all lasted for 3 to 5 days. It resembles Type 2 concerning the spatial distribution of AOD (Figure 11a), although the contamination degree of Type 4 is relatively light, and the mean AOD is 0.63. Over the surface (Figure 11b), the pattern is characterized by the periphery of a high barometric system over Tibetan Plateau. The lack of pressure gradient allows for formation of pollution. At 850hPa (Figure 11c), an anticyclone centered over the study area results in moderate to low wind speed. In the middle troposphere, the circulation is almost zonal passing through mid-latitudes (Figure 11d). Compared to Type 2, the vertical velocity and the divergence, shown in Figures 11e and 11f over East China, respectively, are stronger. Nevertheless, it should be noted that low-level averaged divergence is weaker than that of climatological mean, which are probably the reason why the mean AOD of Type 4 is less than Type 2.

Type 5 (marked with the letter E) depicts a different pattern of pollution distribution. As shown in Figure 12a, the pollutants for Type 5 are gathered in the northeast rather than the center of the studied area. Because the pollutants are not

widespread, the regional mean AOD reaches 0.60 merely. Figure 12 represents the associated circulations. On both surface and 850hPa level, East China is found in the rear zone of the high pressure system located in eastern ocean. Southerly wind dominates in the lower troposphere, while in the middle troposphere, the sparse isopleths indicate small geopotential height gradient. Owing to the weakness in vertical motion ($2.21 \times 10^{-2} \text{ Pas}^{-1}$) and also in the divergence of winds ($1.64 \times 10^{-6} \text{ s}^{-1}$) under such calm weather condition, the pollution is formed. This type occurred for 10% of all polluted days in the sample.

Type 6 (marked with the letter F) consists only one 3-day episode (accounts for 3.3%). Very high AOD values are found in Hunan province, and the averaged AOD over the whole area is 0.70. A surface high pressure system is centered over the Yellow Sea, resulting in southerly flow over the East China, which prevails in the lower troposphere. These conditions contribute to the northward extension of pollutants (Figure 13a). As shown in Figure 13e, the vertical velocity pattern is different from that of other weather types. The descending motion is prevailed in the higher troposphere, while ascending motion in the lower troposphere, transporting some pollutants to higher level. Consequently, we consider the divergence at both low and middle troposphere that are presented in Figure 13f. Despite the divergence of low level is $2.63 \times 10^{-6} \text{ s}^{-1}$, the corresponding value of middle troposphere is merely $0.72 \times 10^{-6} \text{ s}^{-1}$. Thereby, the column AOD is large. Type 6 is usually identified as a “southerly type”.

Similar to the polluted episodes, the results for clean episodes are detailed in the following. The distributions of AOD and the corresponding weather maps for clean

types are shown in Figures 14-16.

Type 7 (marked with the letter G) is the most frequent clean type during the whole examined low-value days (accounts for 57.6%). As shown in Figure 14a, the maximum AOD is less than 0.6. In addition, the mean AOD for the entire region is 0.33, which represents improved air quality in contrast with the above polluted types. According to the circulation pattern of Type 7 (Figure 14), over the surface, cold air moves toward East China continually in front of the high barometric system located in Inner Mongolia. A trough appears in the upper atmosphere, accompanied by an anticyclonic eddy in the lower troposphere, which causes strong northwesterly winds (Figure 14c and d) in the area. When considering the vertical structure of Type 7, as shown in LE, uniformly downward motion with the vertical velocity of $5.78 \times 10^{-2} \text{ Pas}^{-1}$ prevails. Therefore, strong divergence ($2.93 \times 10^{-6} \text{ s}^{-1}$) resulted from wind field in the lower troposphere facilitates the removal of the accumulated pollutants from local areas.

Type 8 (marked with the letter H), which accounts for 18.2% of all clean days, is characterized by a circulation at the rear of weak high pressure system centered in the east coast of China (Figure 15). Corresponding to the pattern on surface, anticyclonic circulations are observed in 850hPa. The vertical downward motion ($2.65 \times 10^{-2} \text{ Pas}^{-1}$) in East China is somewhat stronger than that of climatological mean, whereas the divergence ($3.60 \times 10^{-6} \text{ s}^{-1}$) is much larger than the ten-year average, blowing away local pollutants and bringing clean air from the sea to the region. The above conditions induced a lower mean AOD value of 0.35.

Type 9 (marked with the letter I) is the cleanest type with an averaged AOD value

of 0.31. It is associated with the passage of a cold front, and the occurrence frequency is 24.2%. Over the surface, the high pressure system over the northwest of China, along with a low pressure system centered in northeast of China, intensifies the southward flow of cold air masses, as can be seen in Figure 16. In the lower troposphere, strong northwesterly winds prevail in the region, and the dense isopleths representing for strong geopotential height gradient appears in middle troposphere. Strong descending motion ($6.81 \times 10^{-6} \text{s}^{-1}$) is associated with the whole vertical layers of atmosphere while favorable diffusion condition at low layer is shown in Figure 16f. The advection of cold and dry air from northwest contributes to the good air quality.

In addition, from the above analyses, it can be seen that the temperature fields are particularly indicative of the movement and the intersection of warm and cold air flows. Since the large-scale temperature distribution is closely related to the atmospheric circulations, detailed relationship between AOD and temperature needs further investigation in the future.

4. Discussions

The above nine general circulation types, which are schematically illustrated in Figure 17, correspond to different level of air quality. In Table 1 and 2, it can be found that the two typical cases (HE and LE) correspond to Type 4 and Type 7, respectively. To assess the relationship between diffusion conditions and synoptic patterns in autumn, the values of vertical velocity averaged from 1000hPa to 100hPa and divergence of

wind field in lower troposphere are quantitatively compared among these circulation types (Figure 18). In this study, the climatological means are used as the threshold to discuss the diffusion ability of environment. In general, when the mean downward motion of air is strong over East China with a value larger than $2.56 \times 10^{-2} \text{Pas}^{-1}$, the divergence of low level winds is a predominant factor in deciding the column AOD owing to the accumulation of pollutants in low levels. As shown in Figure 18, for the three polluted types (Type 1, 3, 4), the divergence is less than $1.79 \times 10^{-2} \text{s}^{-1}$, while for three clean types (Type 7, 8, 9) favorable divergent conditions are found. However, Types 2, 5 and 6 are recognized as the types with weak downward motion, in which the aerosols may not be gathered in the lower level. Consequently, it is necessary to account for the convergence of the middle layer due to its modification on the distribution of upper pollutants. In fact, the convergence in upper and divergence in lower levels always appear in autumn, which suggests that the divergence of upper level winds is usually weaker than that of lower level, or even occurring as convergence. For Type 2 and Type 5, the divergence in middle layer are 1.08×10^{-6} and $0.7 \times 10^{-6} \text{s}^{-1}$, respectively, which implies that the divergence of these two types is poor at both low and middle levels. Type 6 is the one with the largest (negative in pressure units) vertical velocity. The upward motion of air in low troposphere transports pollutants to higher levels, and the weak divergence in middle layer ($0.72 \times 10^{-6} \text{s}^{-1}$) leads to the severe pollution.

Admittedly, temporal and spatial variability of air pollution levels are controlled by weather conditions in conjunction with a complex distribution of emission sources. In this study, we suggested that the anthropogenic emission is almost constant in a given

season followed by previous studies (Ziomas et al. 1995; Xu et al. 2011). However, the biomass burning in rural areas may cause an increase in pollution emissions. Therefore, to reduce the sudden influences from biomass burning and confirm the impacts due to atmospheric conditions, we compared the types with almost the same number of fires derived from MODIS active fire product. Although the mean fire numbers for Types 2, 3 and 7 are nearly equal (28, 31 and 26), their corresponding AOD values are different, which is resulted from different weather conditions. The diffusion in Type 7 is the best while in Type 2 it is the worst among these three types (2, 3, and 7) as seen in Figure 18. Similarly, the additional emission from burning is similar for Types 4, 5, and 9, but less than that in the aforementioned three types, since the fire numbers are 20, 15 and 18 respectively. However, the mean AOD for Type 9 is merely half of that for Types 4 and 5 owing to the difference in synoptic patterns. In addition, Types 6 and 8, with fire numbers being 9 and 7, respectively, present exactly opposite air quality, and the pollution of Type 6 is very severe, even though the fire numbers of the two types are relative small compared to other types.

5. Summary and conclusion

In the present study, the climatological mean and interannual variation of AOD over East China (28°N-40°N, 110°E-122°E) are investigated through statistical analysis of ten-year MODIS data (2001-2010). In consideration of weather characteristics in autumn and less variations of pollutants emission during a short time period, October is selected as typical month to study. The air quality during the total 310 days is

represented by the [satellite-measured](#) AOD, and the corresponding meteorological fields [are analyzed using](#) NCEP/NCAR reanalysis dataset. Circulation patterns assessed at three levels (surface, 850hPa and 500hPa) on episode days are identified. The main conclusions are summarized as follows.

[First](#), the daily mean AOD value ranges from 0.3 to 0.7 in large parts of the East China except for four widespread high-value centers, which are considered as possible consequences of constant industrial emissions or agricultural biomass burning. The fluctuation is more volatile over the region where the mean AOD is higher. The circulation patterns [indicate](#) that East China is frequently dominated by large-scale stable circulation [patterns](#) in autumn, such as anticyclonic circulation at 850hPa and northwest flow at 500hPa. Furthermore, since uniform descending motion prevails over the area, which [gathers](#) pollutants together in the lower layer, the divergence of low level wind field plays a key role in determining the column AOD.

Moreover, two distinct extreme episodes, [i.e.](#), LE (October 21st to 24th in 2003) and HE (October 28th to 31st in 2006), are [selected for initial examination of](#) the relations between meteorological [field](#) and air [quality](#). These two episodes showed different circulation patterns at both low and high levels. [Additionally](#), the features of two sets of backward trajectories supported the distinct distributions of AOD associated with [these](#) two episodes. [To](#) get better insight [of](#) the impact of circulation patterns on episodic [pollution](#) events over East China, comprehensive statistics of all 28 episodes occurred in the study period are [computed and analyzed](#). [Among them](#) there are 18 high-value episodes (90 days) and 10 low-value episodes (31 days).

Finally, according to the similarity of circulation patterns [within the](#) 28 episodes [at](#) all the three levels, the 18 pollution episodes are classified into six types, while the other 10 clean episodes are classified into three types. Each type differs from [the](#) other, either in respect to the position and intensity of weather systems or the combination of lower and upper [level](#) atmospheric circulations. Compared [to](#) the polluted types, generally, the flow [in](#) the clean types strengthened significantly [in both middle and lower troposphere](#). These conditions were propitious to the horizontal diffusion of air pollutants. Particularly, patterns that associated with the uniform pressure field in East China, with a steady westerly flow in middle troposphere, or [under](#) the control of an anticyclone are good indications of pollution, while clean episodes occur when strong southeastward cold air advection prevails below the middle troposphere, or air masses are transported from sea to [land](#). The values of vertical velocity and divergence of wind field are effective [indices](#) to [quantitatively identify](#) the differences in diffusion conditions for each type.

In [summary](#), the above results have confirmed the impacts of large-scale atmospheric circulations upon aerosol distributions over East China. Since the empirical classification of weather types are convenient to correlate different circulations patterns with the different air qualities, these results are valuable [for policy-makers to make balanced decisions over economic activity](#) and pollution mitigation.

Acknowledgments. We appreciate the constructive comments and suggestions by the editors and anonymous reviewers. This work is

supported by the NSFC (Grant No. 41230419, 91337213 and 41205126), Special Funds for Public Welfare of China (Grant GYHY201306077), and the Jiangsu Provincial 2011 Program (Collaborative Innovation Center of Climate Change).

References

Al-Saadi, J., Szykman, J., Pierce, R. B., Kittaka, C., Neil, D., Chu, D. A., Remer, L., Gumley, L., Prins, E., Weinstock, L., Macdonald, C., Wayland, R., Dimmick, F. and Fishman, J.: Improving national air quality forecasts with satellite aerosol observations, *B. Am. Meteorol. Soc.*, 86, 1249–1261, 2005.

Borge, R., Lumberras, J., Vardoulakis, S., Kassomenos, P., Rodríguez, E.: Analysis of long-range transport influences on urban PM₁₀ using two-stage atmospheric trajectory clusters, *Atmos. Environ.*, 41, 4434-4450, 2007.

Chen, Z. H., Cheng, S. Y., Li, J. B., Guo, X. R., Wang, W. H., Chen, D. S.: Relationship between atmospheric pollution processes and synoptic pressure patterns in northern China, *Atmos. Environ.*, 42, 6078-6087, 2008a.

Chen, X. L., Fan, S. J., Li J. N., Liu, J., Wang, A. Y., Fong, S. K.: The typical weather characteristics of air pollution in Hong Kong area, *J. Trop. Meteor.*, 24, 195-199, 2008b. (in Chinese)

Chen, Y., Zhao, C., Zhang, Q., Deng, Z., and Huang, M.: Aircraft study of Mountain Chimney Effect of Beijing, China, *J. Geophys. Res.*, 114, D08306,

doi:10.1029/2008JD010610, 2009.

Chen, S. Y., Huang, J. P., Fu, Q., Ge, J. M., Su, J.: Effects of aerosols on autumn precipitation over mid-eastern China, *J. Trop. Meteor.*, 27, 339-347, 2012. (in Chinese)

Chen, B., Stein, A. F., Maldonado, P. G., Sanchez de la Campa, A. M., Gonzalez-Castanedo, Y., Castell, N., de la Rosa, J. D.: Size distribution and concentrations of heavy metals in atmospheric aerosols originating from industrial emissions as predicted by the HYSPLIT model, *Atmos. Environ.*, 71, 234-244, 2013.

Chen, S., Zhao, C., Qian, Y., Leung, L. R., Huang, J., Huang, Z., Bi, J., Zhang, W., Shi, J., Yang, L., Li, D., Li, J.: Regional modeling of dust mass balance and radiative forcing over East Asia using WRF-Chem, *Aeolian Res.*, 15, 15–30, 2014.

Cheng, S. Y., Chen, D. S., Li, J. B., Wang, H. Y., Guo, X. R.: The assessment of emission-source contributions to air quality by using a coupled MM5-ARPS-CMAQ modeling system: a case study in the Beijing metropolitan region, China. *Environ. Modell. Softw.*, 22, 1601-1616, 2007.

Chu, D. A., Kaufman, Y. J., Ichoku, C., Remer, L. A., Tanré, D., and Holben, B. N.: Validation of MODIS aerosol optical depth retrieval over land, *Geophys. Res. Lett.*, 29, 8007, doi:10.1029/2001GL013 205, 2002.

Csavina, J., Field, J., Fdez, O., Corral-Avitia, A. Y., Eduardo S áez, A., Betterton, E. A.: Effect of wind speed and relative humidity on atmospheric dust concentrations in semi-arid climates, *Sci. Total Environ*, 487, 82-90, 2014.

Demuzere, M., Trigo, R. M., Vila-Guerau de Arellano, J., and van Lipzig, N. P. M.: The impact of weather and atmospheric circulation on O₃ and PM₁₀ levels at a rural

mid-latitude site, *Atmos. Chem. Phys.*, 9, 2695-2714, doi:10.5194/acp-9-2695-2009, 2009.

Ding, A. J., Wang, T., Zhao, M., Wang, T., Li, Z.: Simulation of sea-land breezes and a discussion of their implications on the transport of air pollution during a multi-day ozone episode in the Pearl River Delta of China, *Atmos. Environ.*, 38: 6737-6750, 2004.

Ding, A. J., Wang, T., Thouret, V., Cammas, J.-P., and Nédélec, P.: Tropospheric ozone climatology over Beijing: analysis of aircraft data from the MOZAIC program, *Atmos. Chem. Phys.*, 8, 1-13, doi:10.5194/acp-8-1-2008, 2008.

Ding, A. J., Wang, T., Xue, L. K., Gao, J., Stohl, A., Lei, H. C., Jin, D. Z., Ren, Y., Wang, Z. F., Wei, X. L., Qi, Y. B., Liu, J., and Zhang, X. Q.: Transport of north China midlatitude cyclones: Case study of aircraft measurements in summer 2007, *J. Geophys. Res.*, 114, D08304, doi:10.1029/2008JD011023, 2009.

Donaldson, K., Stone, V., Seaton, A., MacNee, W.: Ambient particle inhalation and the cardiovascular system: Potential mechanisms, *Environ. Health. Persp.*, 109, 523-527, 2001.

Draxler, R. R., Hess, G. D.: Description of the HYSPLIT_4 modeling system, NOAA Technical Memorandum ERL ARL-224, 1997.

Flocas, H., Kelessis, A., Helmis, C., Petrakakis, M., Zoumakis, M., Pappas, K.: Synoptic and local scale atmospheric circulation associated with air pollution episodes in an urban Mediterranean area, *Theor. Appl. Climatol.*, 95, 265-277, 2009.

Guo, J. P., Zhang, X. Y., Wu, Y. R., Zhaxi, Y. Z., Che, H. Z., La, B., Wang, W. and Li, X.W.: Spatio-temporal Variation Trends of Satellite-based Aerosol Optical Depth in

- China during 1980-2008, *Atmos. Environ.*, 45, 6802–6811, 2011.
- Guo, Y. F., Li, D. Y., Zhou, B., Xia, J., Wu, Y., Hu, Y. H.: Study on haze characteristics in Wuxi and its impact factors, *Meteor. Mon.*, 39, 1314-1324, 2013. (in Chinese)
- He, Q. S., Li, C. C., Geng, F. H., Lei, Y., Li, Y. H.: Study on long-term aerosol distribution over the land of east China using MODIS data, *Aerosol Air Qual. Res.*, 12, 304-319, 2012.
- Janssen, N. A., Hoek G., Simic-Lawson. M., Fischer, P., van Bree, L., ten Brink, H., Keuken, M., Atkinson, R. W., Anderson, H. R., Brunekreef, B. and Cassee, F. R.: Black carbon as an additional indicator of the adverse health effects of airborne particles compared with PM₁₀ and PM_{2.5}, *Environ. Health. Persp.*, 119, 1691–1699, 2011.
- Kan, H., Chen, B.: Particulate air pollution in urban areas of Shanghai, China: health-based economic assessment, *Sci. Total Environ.*, 322, 71–79, 2004.
- Kassomenos, P. A., Sindosi, O. A., Lolis, C. J. and Chaloulakou, A.: On the relation between seasonal synoptic circulation types and spatial air quality characteristics in Athens, Greece, *J. Air. Waste. Manage.*, 53, 309–324, 2003.
- Kaufman, Y. J., Tanre, D. and Boucher O.: A satellite view of aerosols in the climate system, *Nature*, 419, 215–223, 2002.
- Kim, S. W., Yoon, S. C., Kim, J. Y. and Kim, S. Y.: Seasonal and monthly variations of columnar aerosol optical properties over East Asia determined from multi-year MODIS, LIDAR, and AERONET sun/sky radiometer measurements, *Atmos. Environ.*, 41, 1634–1651, 2007.
- Koren, I., Altaratz, O., Remer, L. A., Feingold, G., Martins, J. V., Heiblum, R. H.:

Aerosol-induced intensification of rain from the tropics to the mid-latitudes, *Nat. Geosci.*, 5(2): 118-122, doi: 10.1038/NGEO1364, 2012.

Li, Z. Q., Niu, F., Fan, J. W., Liu, Y. G., Rosenfeld, D., Ding, Y. N.: Long-term impacts of aerosols on the vertical development of clouds and precipitation, *Nat. Geosci.*, 4(12): 888-894, doi: 10.1038/NGEO1313, 2011.

Lin, J., Nielsen, C. P., Zhao, Y., Lei, Y. Liu, Y. and Mcelroy, M. B.: Recent changes in particulate air pollution over China observed from space and the ground: effectiveness of emission control, *Environ. Sci. and Technol.*, 44, 7771–7776, 2010.

Liu, Y. K., Liu, J. F., Tao, S.: Interannual variability of summertime aerosol optical depth over East Asia during 2000–2011: a potential influence from El Niño Southern Oscillation, *Environ. Res. Lett.*, 8, 044034 , 2013.

Luo, Y. X., Zheng, X. B., Zhao, T. L., Chen, J.: A climatology of aerosol optical depth over China from recent 10 years of MODIS remote sensing data, *Int. J. Climatol.*, 34, 863-870, 2014.

Rosenfeld, D., Cattani, E., Melani, S., Levizzani, V.: Considerations on Daylight Operation of 1.6-VERSUS 3.7- μm Channel on NOAA and Metop Satellites, *Bull. Amer. Meteor. Soc.*, 85(6): 873-881, 2004.

Rosenfeld, D., Dai, J., Yu, X., Yao, Z. Y., Xu, X. H., Yang, X., Du, C. L.: Inverse relations between amounts of air pollution and orographic precipitation, *Science*, 315(5817), 1396-1398, 2007

Russo, A., Trigo, R. M., Martins, H., Mendes, M. T.: NO₂, PM₁₀ and O₃ urban concentrations and its association with circulation weather types in Portugal, *Atmos.*

Environ., 89, 768-785, 2014.

Saavedra, S., Rodríguez, A., Taboada, J. J., Souto, J. A., Casares, J. J.: Synoptic patterns and air mass transport during ozone episodes in northwestern Iberia, *Sci. Total Environ.*, 441, 97-110, 2012.

Shahgedanova, M., Burt, T. P., Davies, T. D.: Synoptic climatology of air pollution in Moscow, *Theor. appl. climatol.*, 61, 85-102, 1998.

Tanner, P. A., Law, P. T.: Effects of synoptic weather systems upon the air quality in an Asian megacity, *Water Air Soil Poll*, 136, 105-124, 2002.

Twohy, C. H., Coakley, J. A. and Tahnk, W. R.: Effect of changes in relative humidity on aerosol scattering near clouds, *J. Geophys. Res.*, 114, D05205, doi:10.1029/2008JD010991, 2009.

Twomey S.: The influence of pollution on the shortwave albedo of clouds, *J. Atmos. Sci.*, 34(7), 1149-1152, 1977.

Wang, X. Q., Qi, Y. B., Wang, Z. F., Guo, H., Yu, T.: The influence of synoptic pattern on PM₁₀ heavy air pollution in Beijing, *Climatic Environ. Res.*, 12, 81-86, 2007. (in Chinese)

Wang, S. X., Zhang, C. Y.: Spatial and temporal distribution of air pollutant emissions from open burning of crop residues in China, *Sciencepaper Online*, 3, 329-333, 2008. (in Chinese)

Wang, J., Li, J. L., Zhang Y. H.: Weather situation classification and its feature in severe air pollution days in winter in Urumqi, *J. Meteor. Environ.*, 29, 28-32, 2013. (in Chinese)

Wu, J., Guo, J., Zhao, D. M.: Characteristics of aerosol transport and distribution in

East Asia, Atmos. Res., 132, 185-198, 2013.

Xin, J. Y., Zhang, Q., Wang, L. L., Gong, C. S., Wang, Y. S., Liu, Z. R. and Gao, W. K.: The empirical relationship between the PM 2.5 concentration and aerosol optical depth over the background of North China from 2009 to 2011, Atmos. Res., 138, 179-188, 2014.

Xu, W. Y., Zhao, C. S., Ran, L., Deng, Z. Z., Liu, P. F., Ma, N., Lin, W. L., Xu, X. B., Yan, P., He, X., Yu, J., Liang, W. D., and Chen, L. L.: Characteristics of pollutants and their correlation to meteorological conditions at a suburban site in the North China Plain, Atmos. Chem. Phys., 11, 4353-4369, doi:10.5194/acp-11-4353-2011, 2011.

Yang, Y. J., Fu, Y. F., Wu, B. W., Shi, C. E., Deng, X. L., Zhang, H., Zhang, Y.: Impacts of Agricultural Fire on Aerosol Distribution over East China during Summer Harvest time, Journal of Atmospheric and Environmental Optics., 8(4): 241-252, 2013. (in Chinese)

Zhang, L., Liao, H., Li, J. P.: Impacts of Asian summer monsoon on seasonal and interannual variations of aerosols over eastern China, J. Geophys. Res., 115, D00K05, doi:10.1029/2009JD012299, 2010.

Zhao, C., Wang, Y., Yang, Q., Fu, R., Cunnold, D., Choi, Y.: Impact of East Asian summer monsoon on the air quality over China: View from space, J. Geophys. Res., 115, D09301, doi:10.1029/2009JD012745, 2010.

Zhao, C., Liu, X., Leung, L. R.: Impact of the Desert dust on the summer monsoon system over Southwestern North America, Atmos. Chem. Phys., 12, 3717-3731, 2012.

Zhao, C., Leung, L. R., Easter, R., Hand, J., Avise, J.: Characterization of speciated

aerosol direct radiative forcing over California, *J. Geophys. Res.*, 118, 2372–2388, doi:10.1029/2012JD018364, 2013a.

Zhao, C., Liu, X., Qian, Y., Lin, G., McFarlane, S., Yoon, J., Wang, H., Hou, Z., Yang, B., Ma, P., Yan, H., Bao, J.: Sensitivity of Radiative Fluxes at Top of Atmosphere to Cloud-Microphysics and Aerosol Parameters in the Community Atmosphere Model (CAM5), *Atmos. Chem. Phys.*, 13, 10969-10987, 2013b.

Zhao, C. S., Tie, X. X., Lin, Y. P.: A possible positive feedback of reduction of precipitation and increase in aerosols over eastern central China, *Geophys. Res. Lett.*, 33, L11814, doi:10.1029/2006GL025959, 2006a.

Zhao, C. S., Tie, X. X., Brasseur, G., Noone, K. J., Nakajima, T., Zhang, Q., Zhang, R. Y., Huang, M. Y., Duan, Y., Li, G. L., and Ishizaka, Y.: Aircraft measurements of cloud droplet spectral dispersion and implications for indirect aerosol radiative forcing, *Geophys. Res. Lett.*, 33, L16809, doi:10.1029/2006GL026653, 2006b.

Ziomas, I., Melas, D., Zerefos, C., Bais, A., Paliatso, A.: Forecasting peak pollutant levels from meteorological variables, *Atmos. Environ.*, 29, 3703-3711, 1995.

Tables and captions

Table 1. [Descriptions](#) of observed meteorological field features for the 18 pollution episodes (The rows in the table with same capital letters in the parentheses indicate those episodes are affected by the similar circulation patterns in all the three atmospheric levels.)

episodes	Year(Date)	Surface	850hPa	500hPa
1(A)	2002(01-04)	Before the passage of a cold front	strong cold wind blow to south	NW flow
2(B)	2002(08-16)	Uniform pressure field	the rear of anticyclone	W-NW flow
3(C)	2002(24-26)	Periphery of the high pressure system centered in the Mongolia	the foreside of anticyclone	NW flow (behind the trough)
4(C)	2004(07-13)	Periphery of the high pressure system centered in the Mongolia	the foreside of anticyclone	NW flow (behind the trough)
5(D)	2004(18-22)	Periphery of the high pressure system centered in the TP	anticyclonic circulation	W flow
6(F)	2004(27-29)	The rear of high pressure system	South wind	SW flow
7(D)	2005(16-18)	Periphery of the high pressure system centered in the TP	anticyclonic circulation	Shallow trough
8(E)	2005(23-26)	The rear of high pressure system	the rear of anticyclone	W-NW flow
9(B)	2006(04-15)	Uniform pressure field	the rear of anticyclone	W-NW flow
10(D)	2006(28-31)	Periphery of the high pressure system centered in the TP	the foreside of anticyclone	Shallow trough
11(B)	2007(16-25)	Uniform pressure field	anticyclonic circulation	W-NW flow
12(B)	2008(01-03)	Uniform pressure field	the rear of anticyclone	NW flow
13(E)	2008(13-17)	The rear of high pressure system	the rear of anticyclone	W-NW flow
14(C)	2009(02-06)	Periphery of the high pressure system centered in the Mongolia	the foreside of anticyclone	NW flow (behind the trough)
15(A)	2009(15-16)	Before the passage of a cold front	strong cold flow toward south	NW flow
16(D)	2009(21-25)	Periphery of the high pressure system centered in the TP	anticyclonic circulation	W flow
17(B)	2010(16-17)	Periphery of the high pressure system centered in the Mongolia	the rear of anticyclone	NW flow
18(C)	2010(28-31)	Periphery of the high pressure system centered in the Mongolia	the foreside of anticyclone	NW flow (behind the trough)

Table 2. As in Table 1, but for 10 [clean](#) episodes

episodes	Year(Date)	Surface	850hPa	500hPa
1(G)	2001(10-11)	Periphery of the high pressure system	anticyclonic circulation	NW flow (behind the trough)
2(H)	2001(29-30)	the rear of high pressure system	anticyclonic circulation	W flow
3(G)	2003(15-18)	Periphery of the high pressure system	the foreside of anticyclone, strong wind	NW flow
4(G)	2003(21-24)	Periphery of the high pressure system	the foreside of anticyclone, strong wind	NW flow
5(G)	2003(27-28)	Periphery of the high pressure system	the foreside of anticyclone, strong wind	NW flow
6(G)	2004(02-04)	Uniform pressure field	anticyclonic circulation	NW flow (behind the trough)
7(H)	2005(08-10)	the rear of high pressure system	anticyclonic circulation	W flow
8(I)	2008(23-26)	The passage of cold front	strong cold wind	NW flow
9(I)	2009(17-20)	The passage of cold front	strong cold wind	NW flow
10(G)	2010(03-04)	Periphery of the high pressure system	anticyclonic circulation, strong wind	NW flow (behind the trough)

Figures and captions

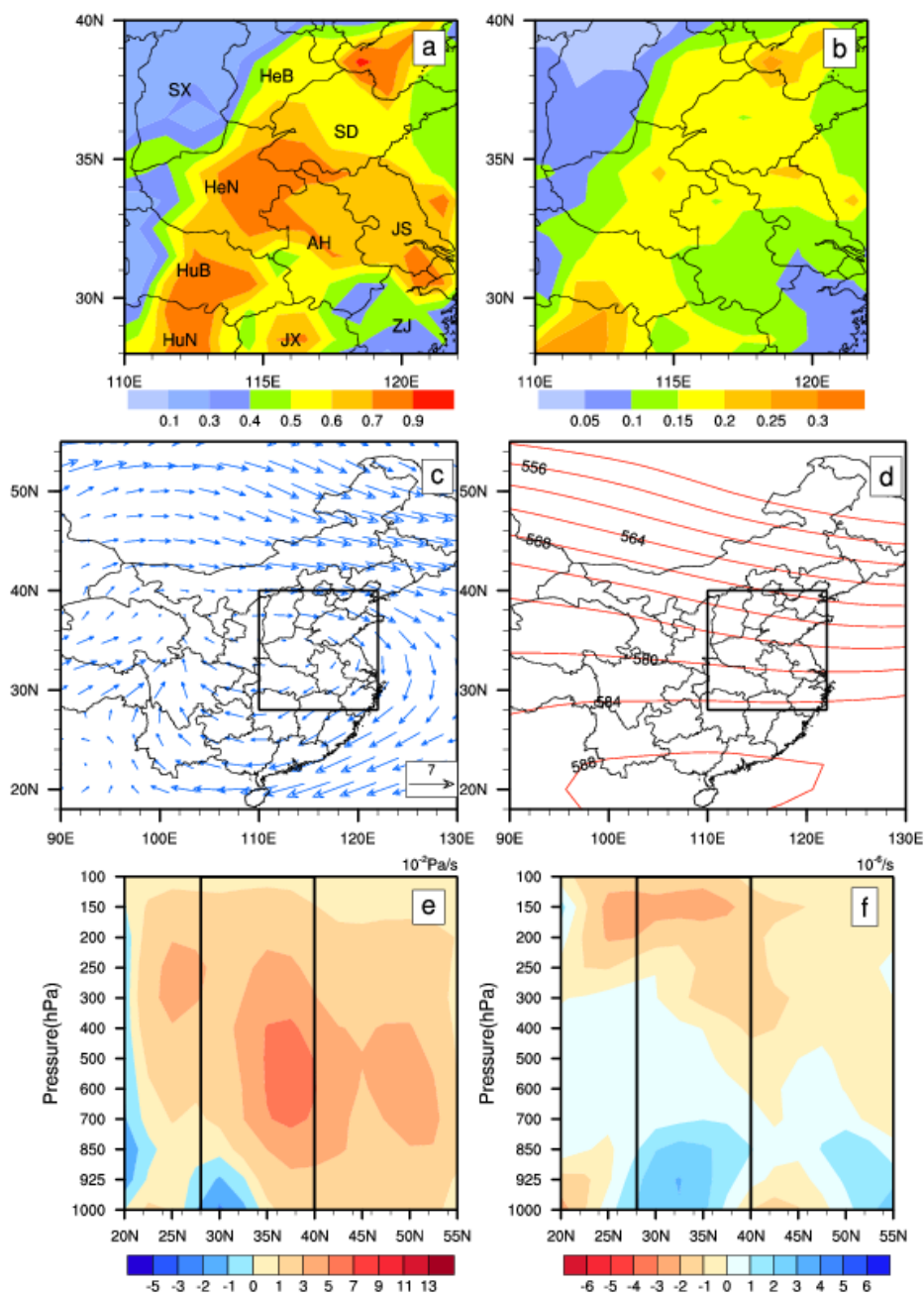


Fig.1. The mean distribution of (a) aerosol optical depth (AOD), (b) the standard deviation of AOD, (c)850hPa winds field, (d) 500hPa geopotential height field, (e) height-latitude cross-sections of vertical velocity (10^{-2} Pa/s) and (f) divergence of winds (10^{-6} /s) averaged from longitude of 110°E - 122°E in October for the period from 2001 to 2010. Black letters on Fig.1(a) indicate the different provinces. SX: Shanxi; SD: Shandong; HeB: Hebei; HeN: Henan; HuB: Hubei; HuN: Hunan; AH: Anhui; JX: Jiangxi; JS: Jiangsu; ZJ: Zhejiang.) Note: (c)- (f) indicate the circulations over East Asia (18°N - 55°N , 90°E - 130°E .) and black rectangular regions in this and subsequent figures represent the East China (28°N - 40°N , 110°E - 122°E) region where this study is focused on.

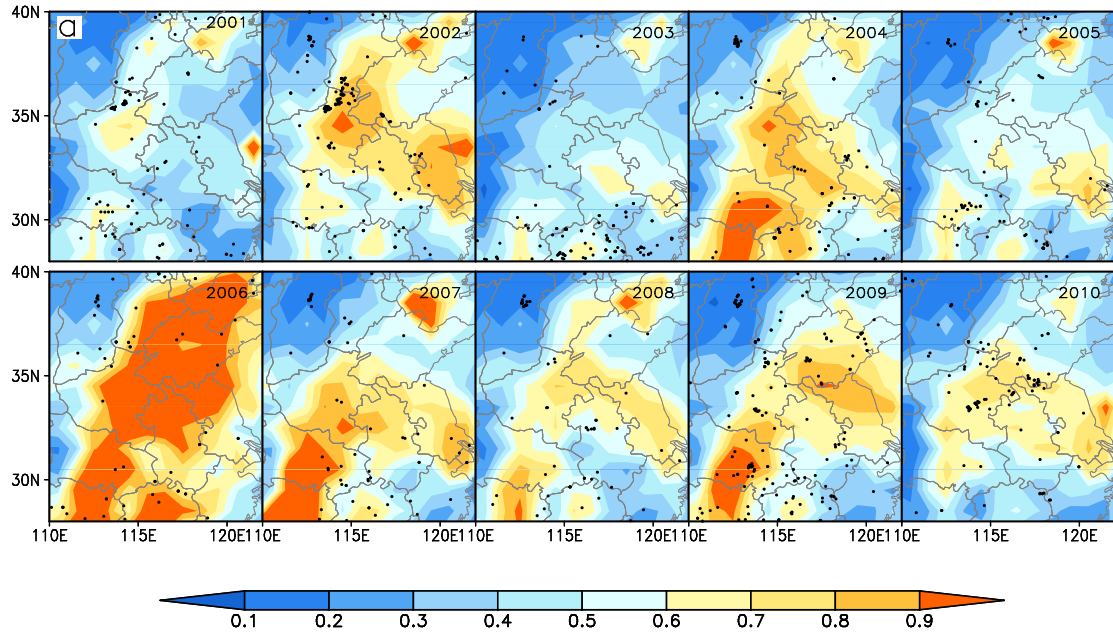


Fig. 2a. The distribution of AOD over East China in October for 2001-2010. The black dots are fire locations .

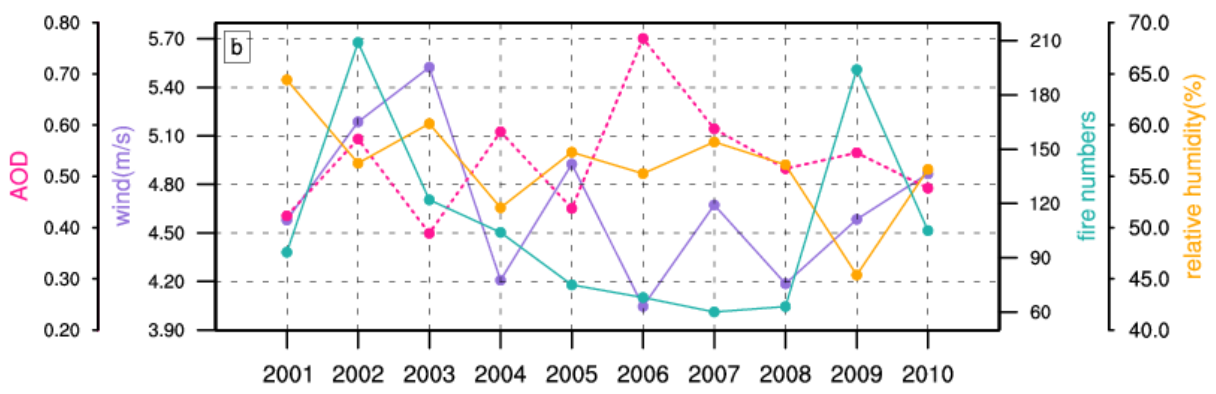


Fig.2b. Interannual variability of column AOD (peach). Fire numbers are in green. Wind speed (purple) and relative humidity (orange) are averages in the lower troposphere (1000hPa-850hPa) and over the region shown in 2a.

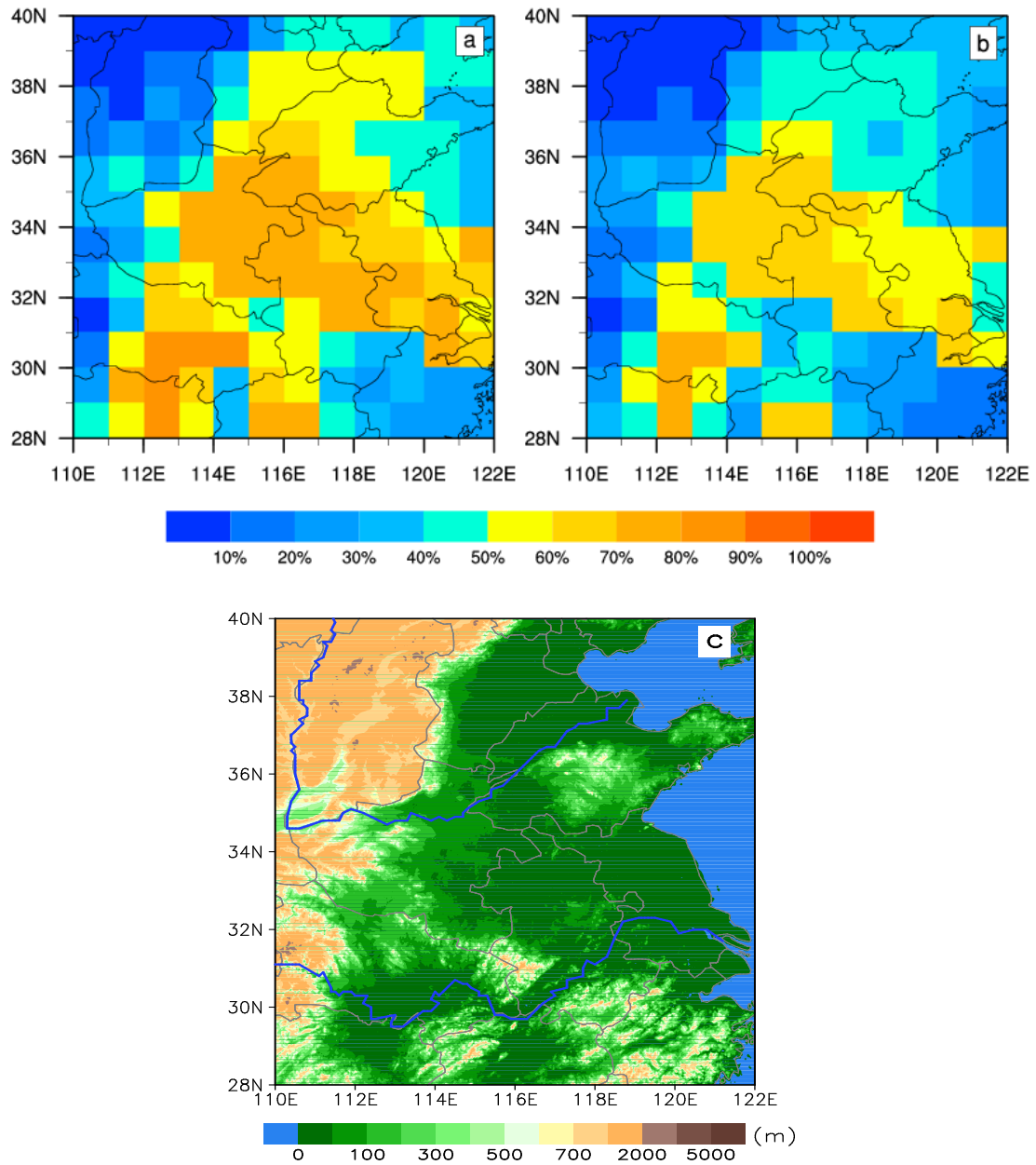


Fig.3. Frequency distribution of (a) AOD>0.5 and (b) AOD>0.6 in October calculated from 2001 to 2010, and (c) the topography of East China.

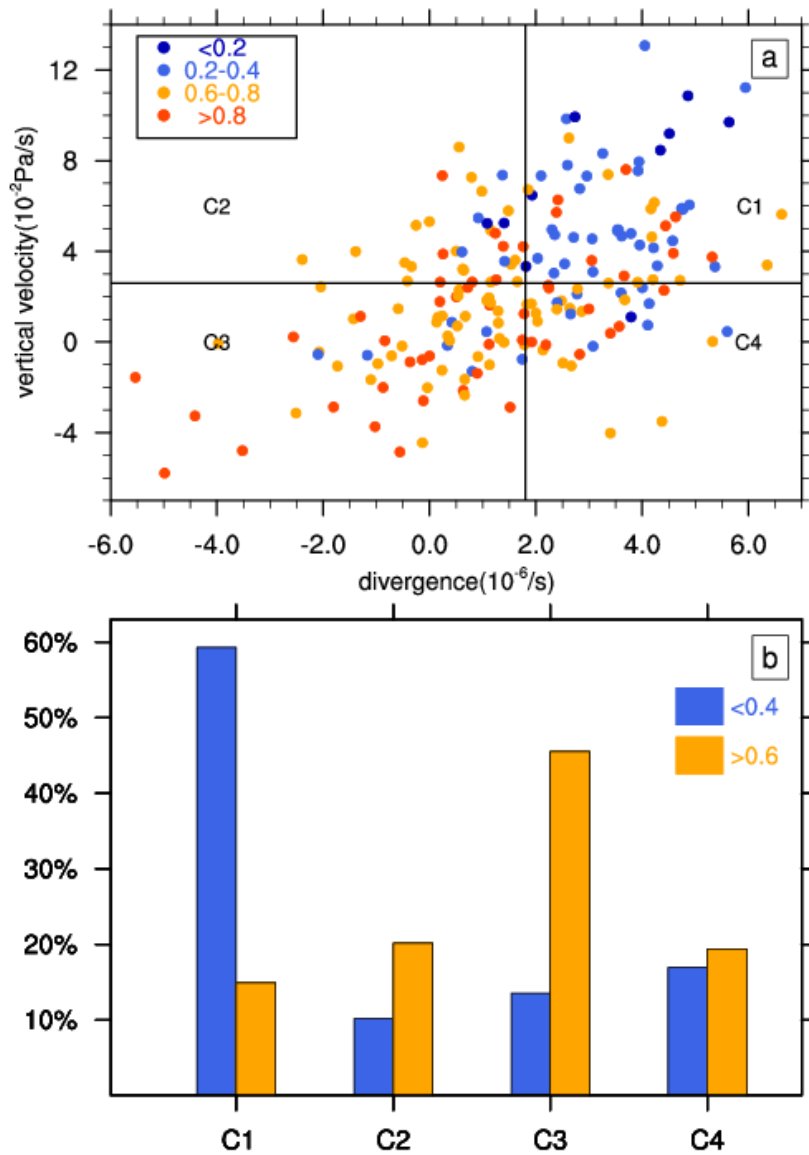


Fig. 4. (a) Dependence of AOD on vertical velocity ($V:10^{-2}\text{Pa s}^{-1}$) averaged from 1000hPa to 100hPa and divergence of wind field ($D: 10^{-6}\text{s}^{-1}$) averaged from 1000hPa to 850hPa. The vertical black line stands for the climatological mean divergence ($1.79 \times 10^{-6}\text{s}^{-1}$) and the horizontal line represents for that of vertical velocity ($2.56 \times 10^{-2} \text{ Pa s}^{-1}$). The samples are divided into four categories according to these two parameters, i.e., C1 ($D > 1.79 \times 10^{-6}$; $V > 2.56 \times 10^{-2}$); C2 ($D < 1.79 \times 10^{-6}$; $V > 2.56 \times 10^{-2}$); C3 ($D < 1.79 \times 10^{-6}$; $V < 2.56 \times 10^{-2}$); C4 ($D > 1.79 \times 10^{-6}$; $V < 2.56 \times 10^{-2}$). (b) Frequency distribution of AOD >0.6 and AOD <0.4 for each category.

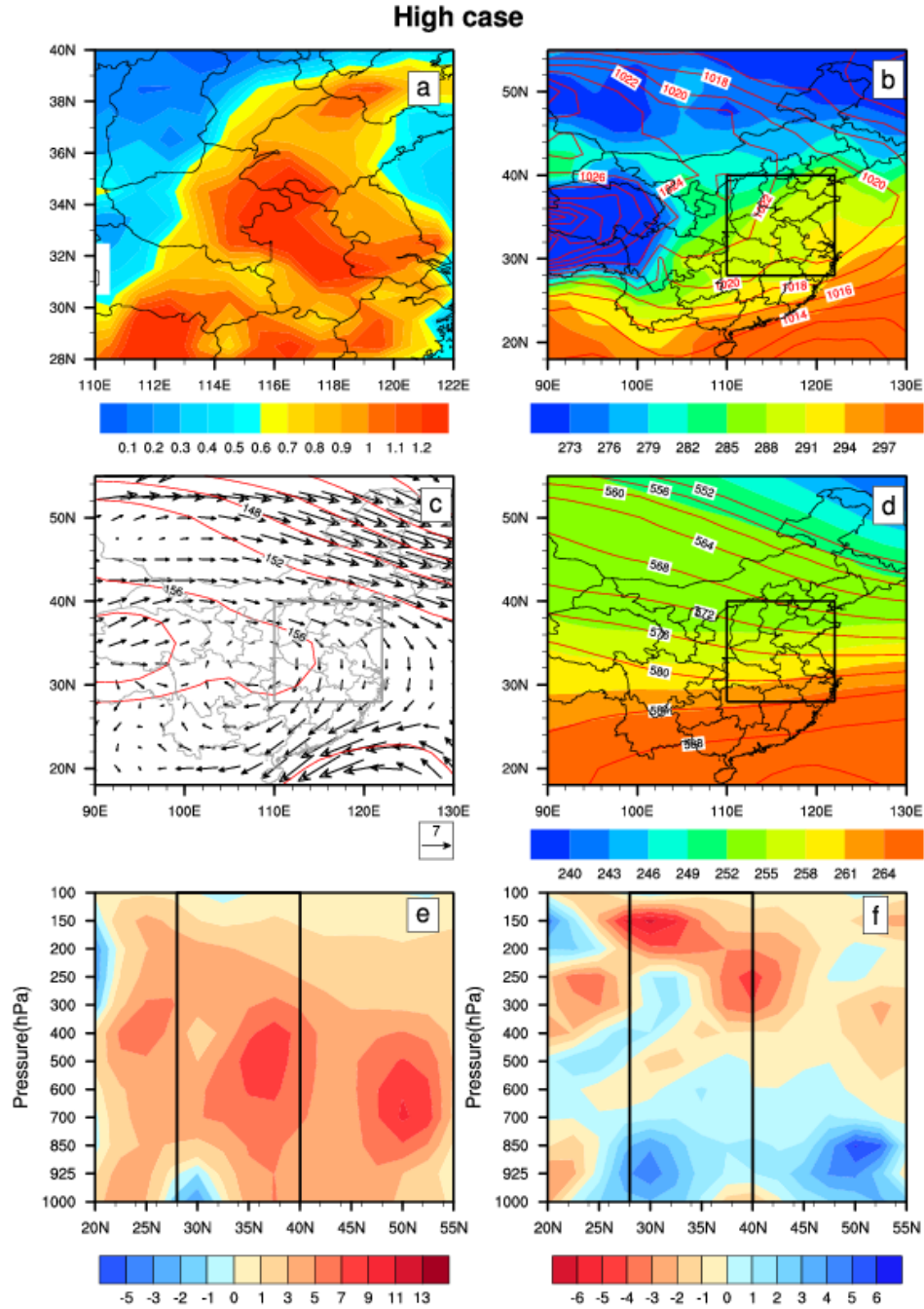


Fig. 5. A typical polluted episode (28th.Oct.2006 to 31st.Oct.2006). (a) The distribution of AOD over East China, (b) sea level pressure (red line) and temperature (color shades) fields, (c) 850hPa wind and geopotential height (red line) fields, (d) 500hPa temperature (color shades) and geopotential height (red line) fields, (e) height-latitude cross-sections of vertical velocity (10^{-2} Pa per second), and (f) divergence of winds (10^{-6} per second) averaged from longitude of 110°E - 122°E . Note: black rectangular region represents the East China (110°E - 122°E , 28°N - 40°N).

Low case

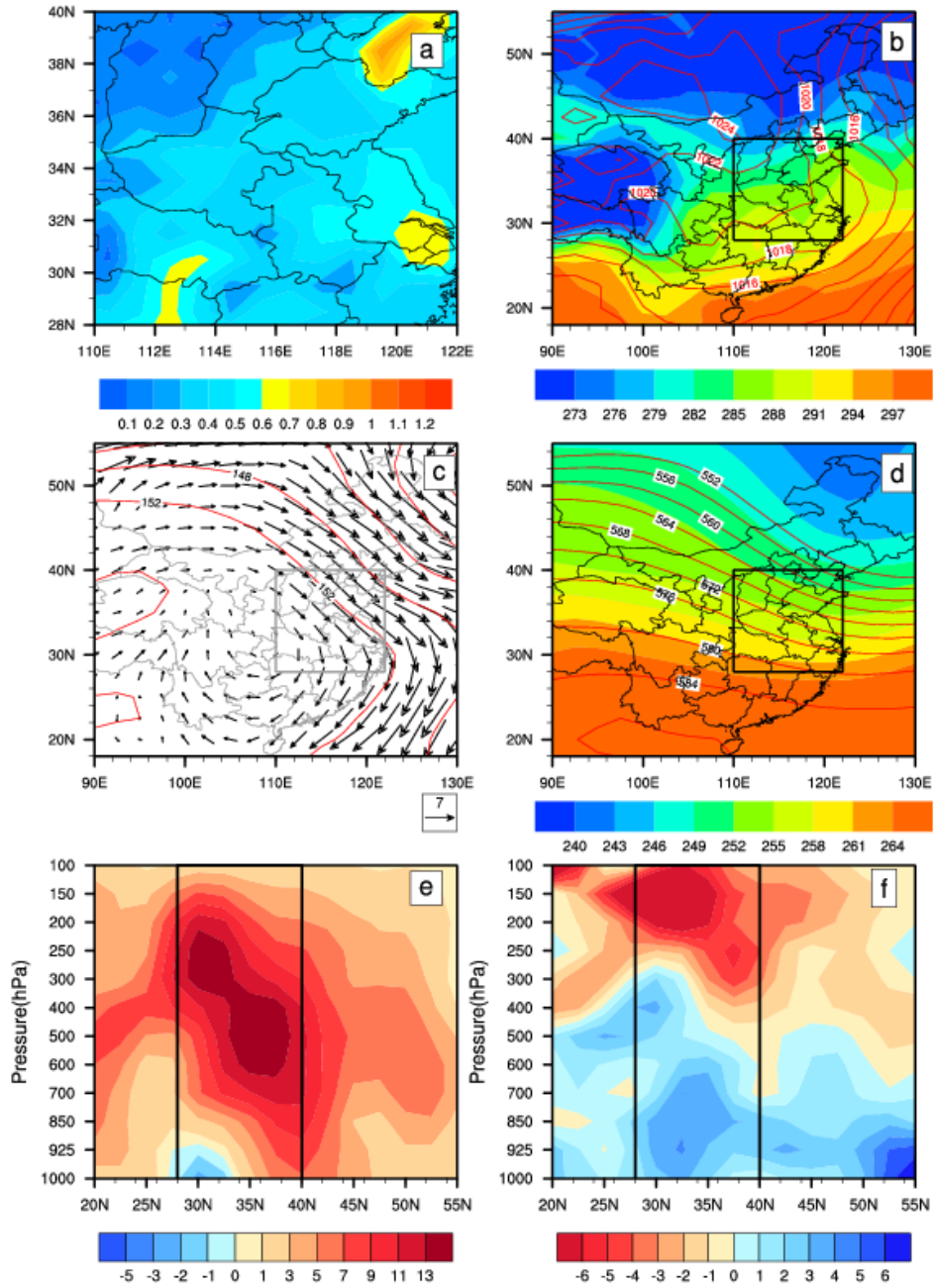


Fig. 6. As in Fig.5, but for the clean episode (21st.Oct.2003 to 24th.Oct.2003)

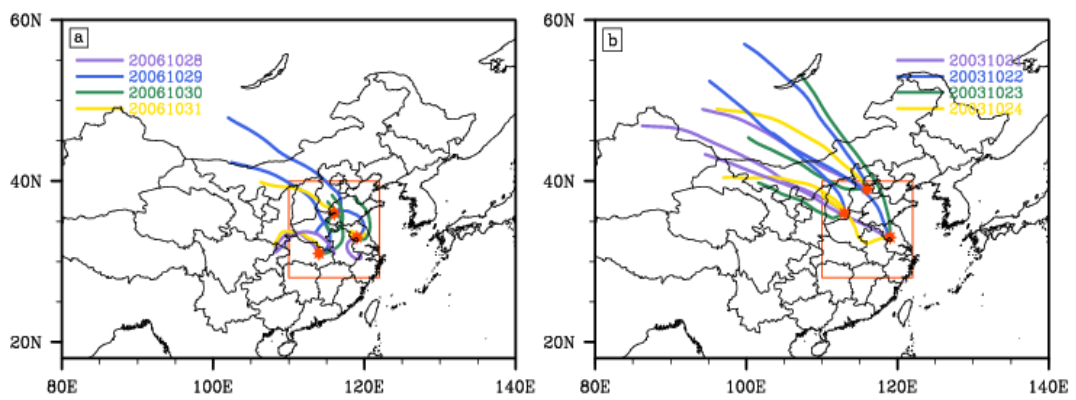


Fig. 7. The 48-hour backward trajectories for two episodes over East China (red box), three red star represent three ending points. (a) Polluted episode, at 31 N,114 E; 33 N,119 E; 36 N,116 E. (b) Clean episode, at 33 N,119 E; 36 N,113 E; 39 N,116 E.

Type 01

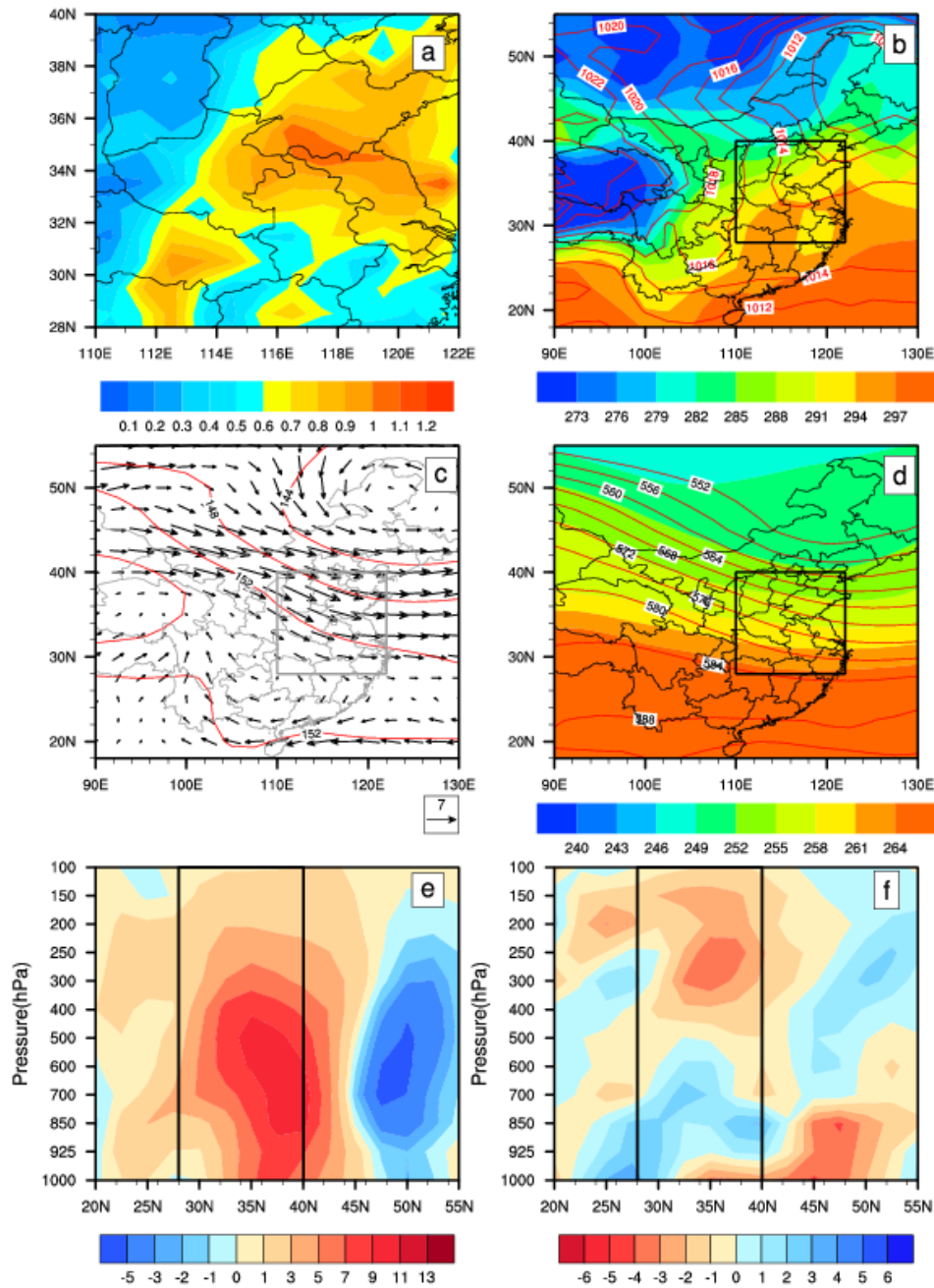


Fig. 8. Type 1 (polluted). (a) The distribution of AOD over East China, (b) sea level pressure (red line) and temperature (color shades) fields, (c) 850hPa wind field and geopotential height (red line) fields, (d) 500hPa temperature (color shades) and geopotential height (red line) fields, (e) height-latitude cross-sections of vertical velocity (10^{-2} Pa per second), and (f) divergence of winds (10^{-6} per second) averaged from longitude of 110°E-122°E. Note: black rectangular region represents the East China (110°E-122°E, 28°N-40°N).

Type 02

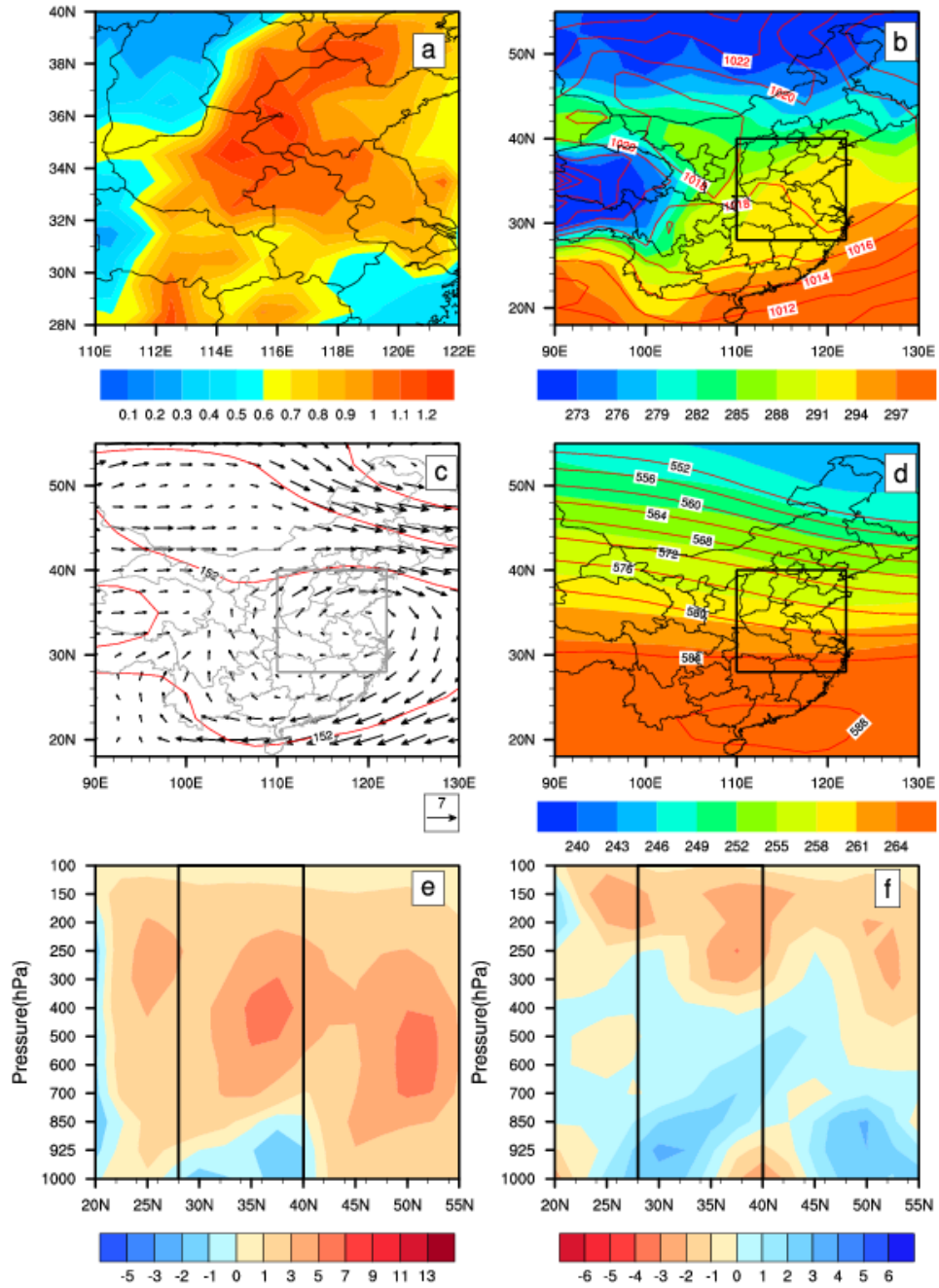


Fig. 9. As in Fig.8, but for Type 2 (polluted).

Type 03

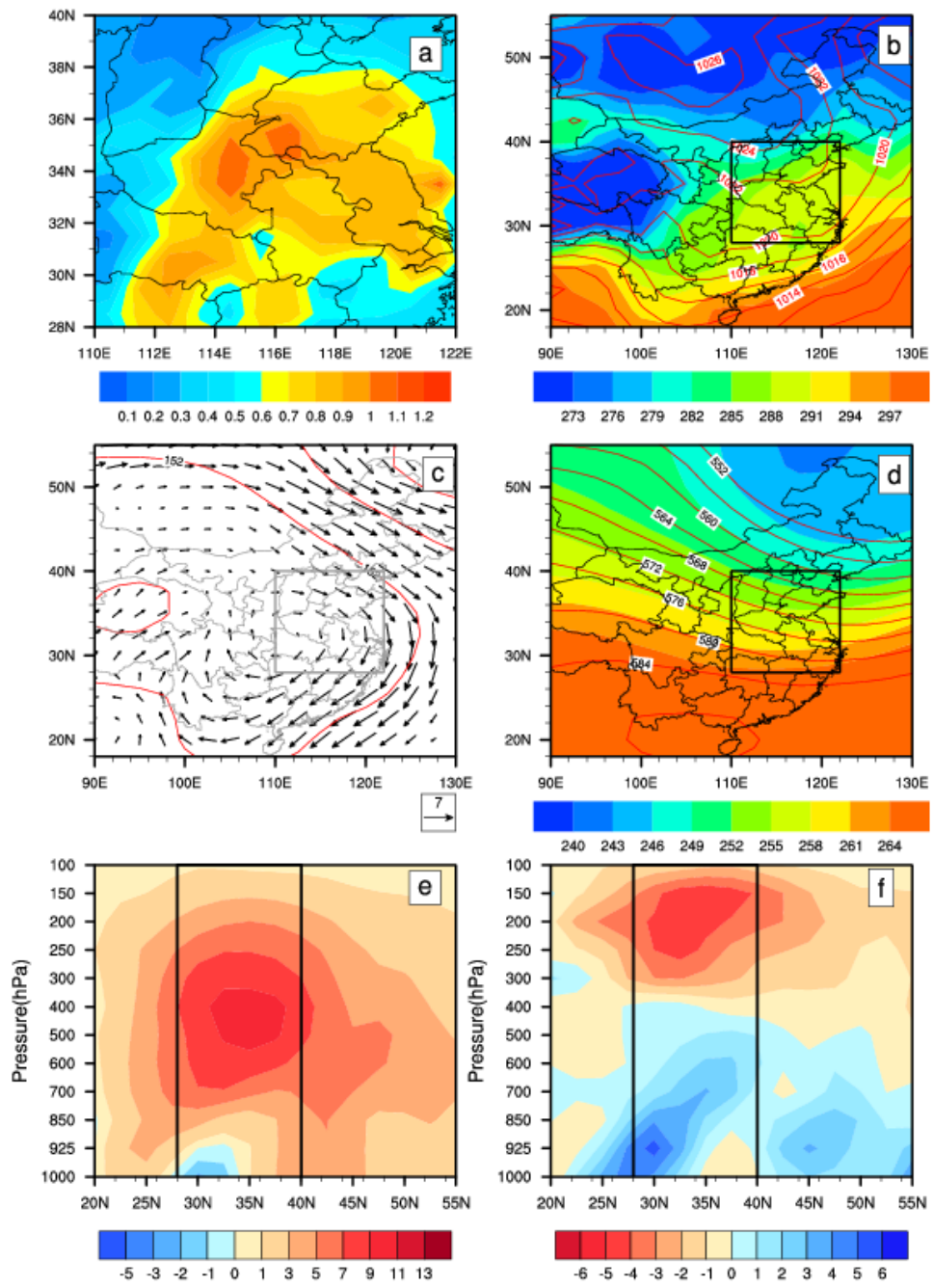


Fig. 10. As in Fig.8, but for Type 3 (polluted).

Type 04

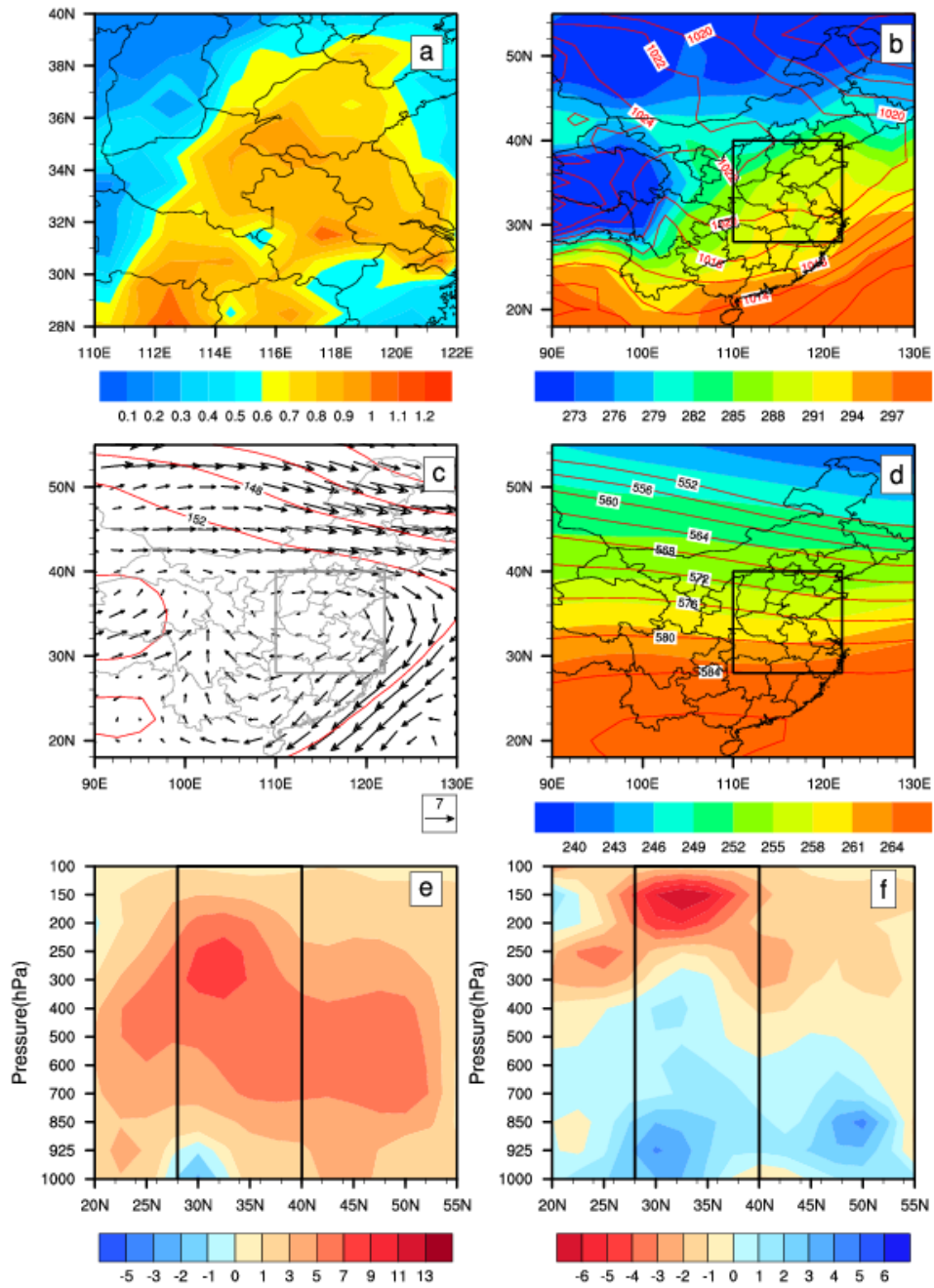


Fig.11. As in Fig.8, but for Type 4 (polluted).

Type 05

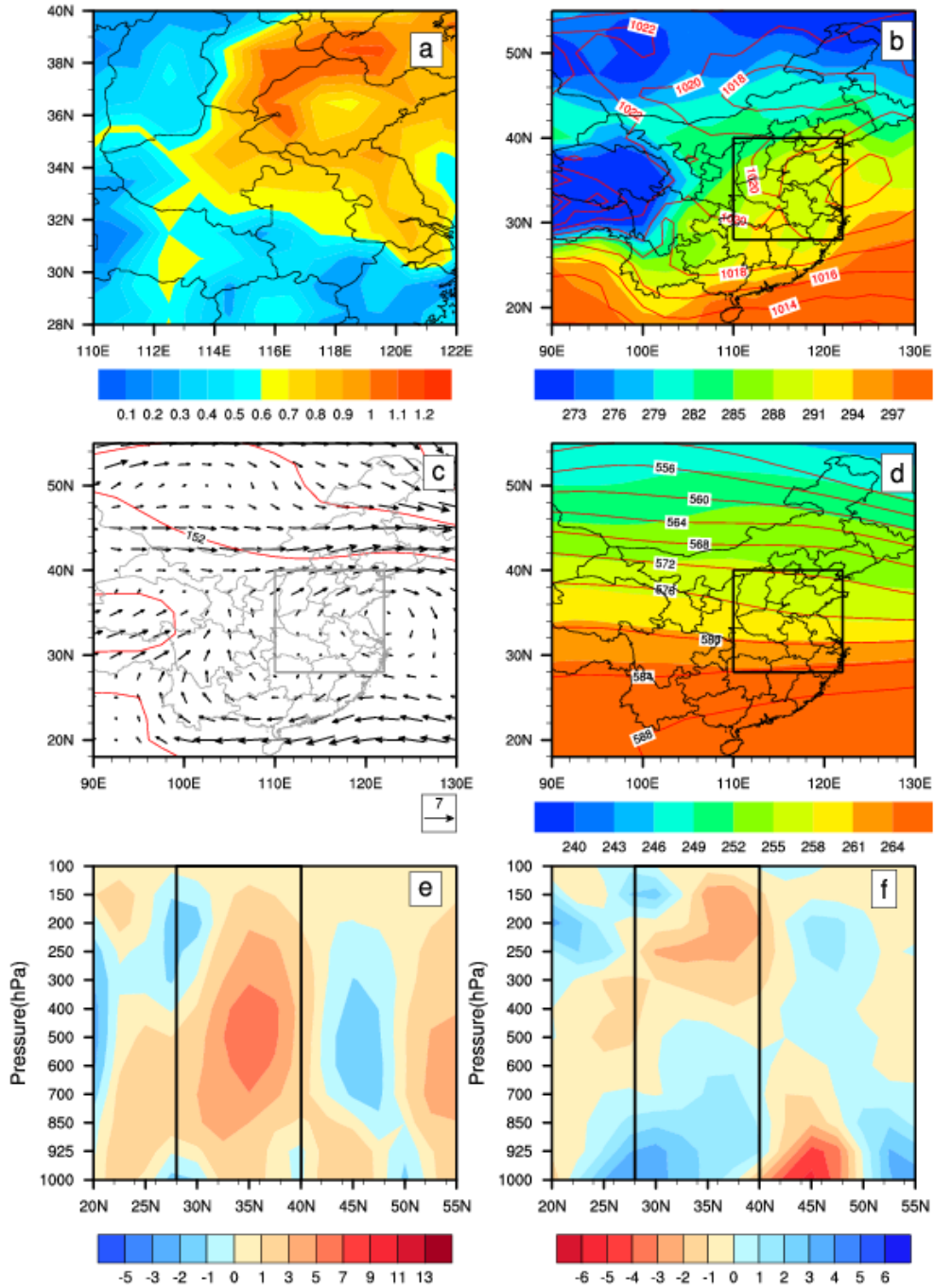


Fig.12. As in Fig.8, but for Type 5 (polluted).

Type 06

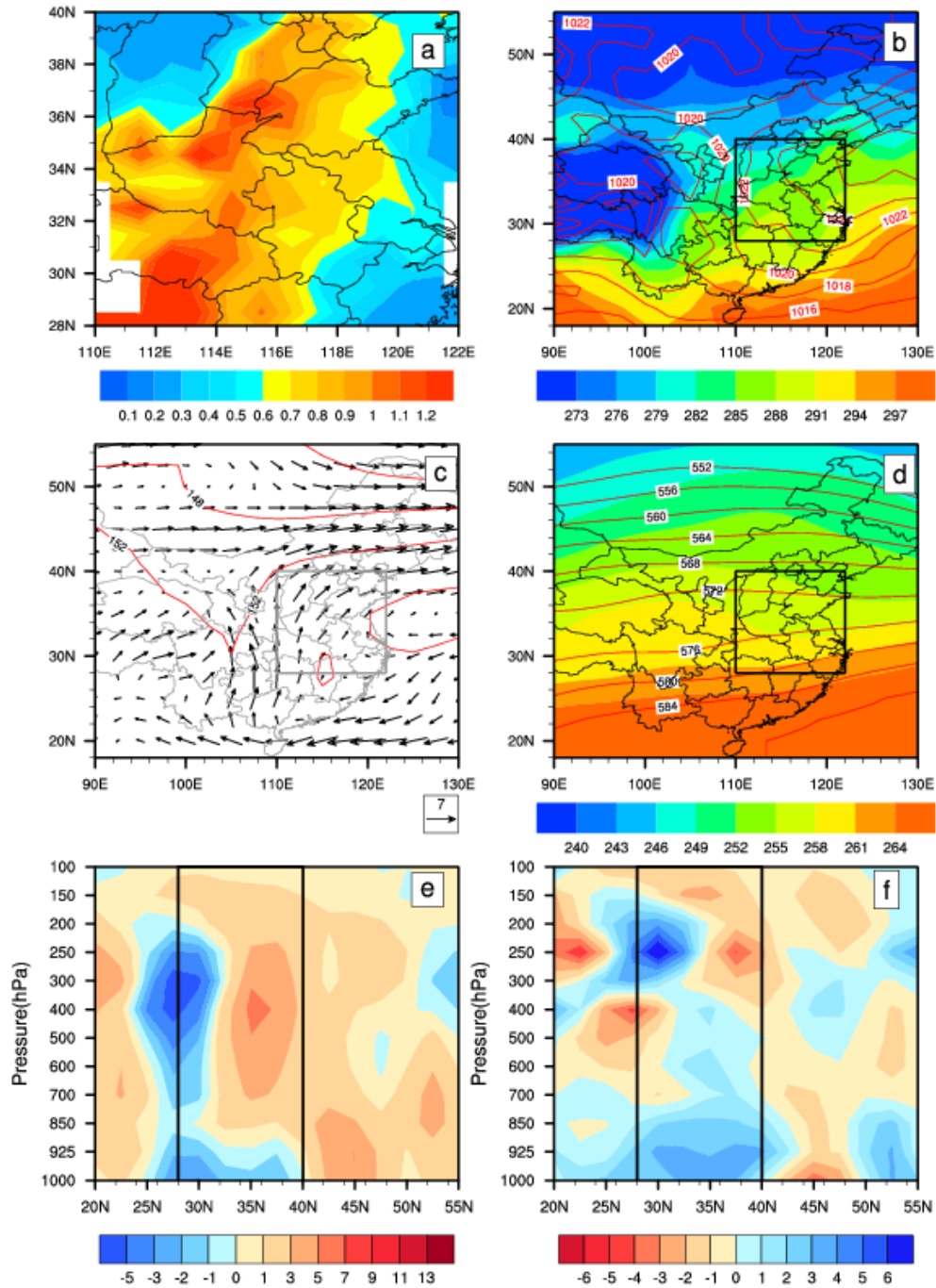


Fig.13. As in Fig.8, but for Type 6 (polluted).

Type 07

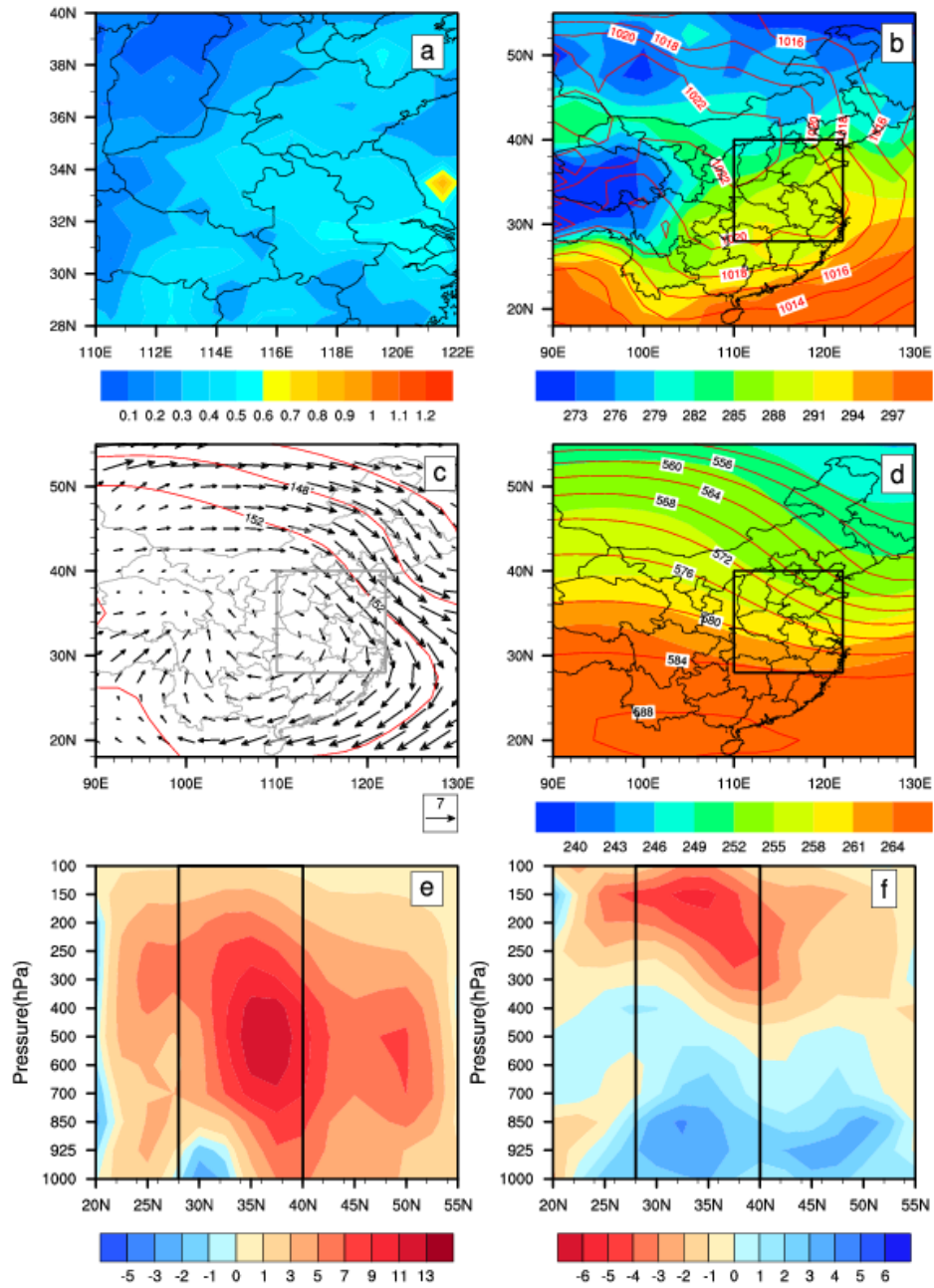


Fig.14. As in Fig.8, but for Type 7 (clean).

Type 08

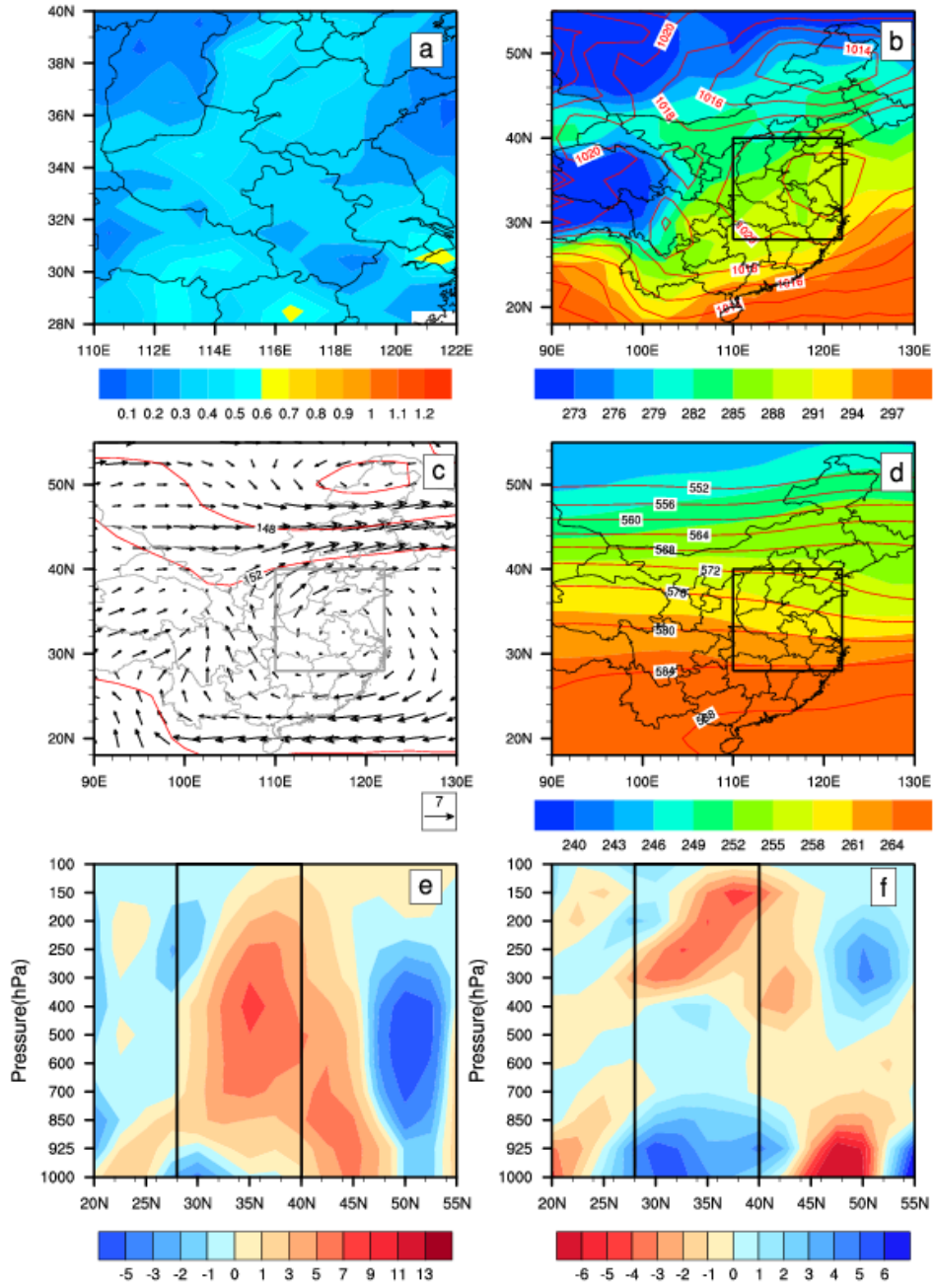


Fig.15. As in Fig.8, but for Type 8 (clean).

Type 09

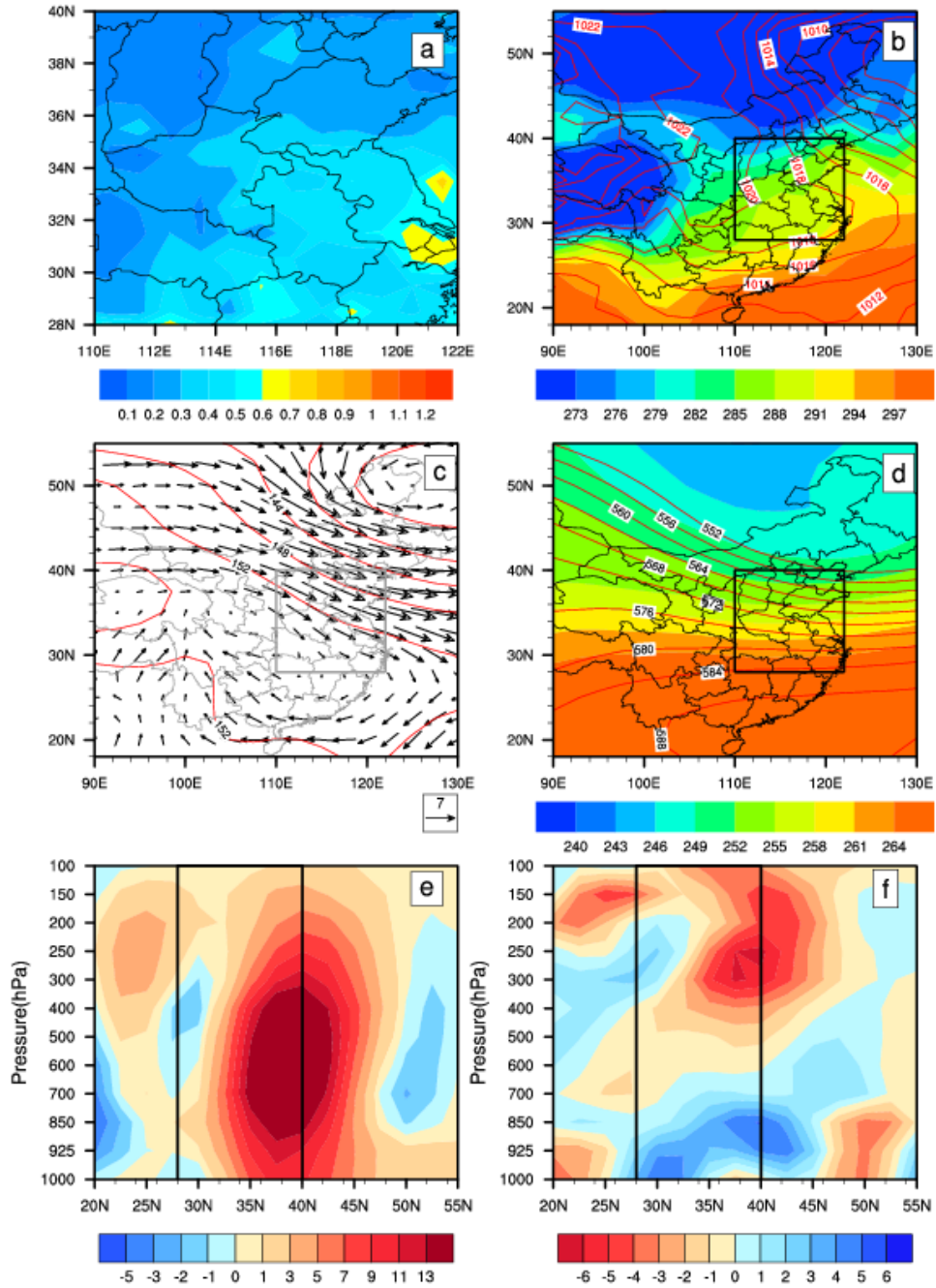


Fig.16. As in Fig. 8, but for Type 9 (clean).

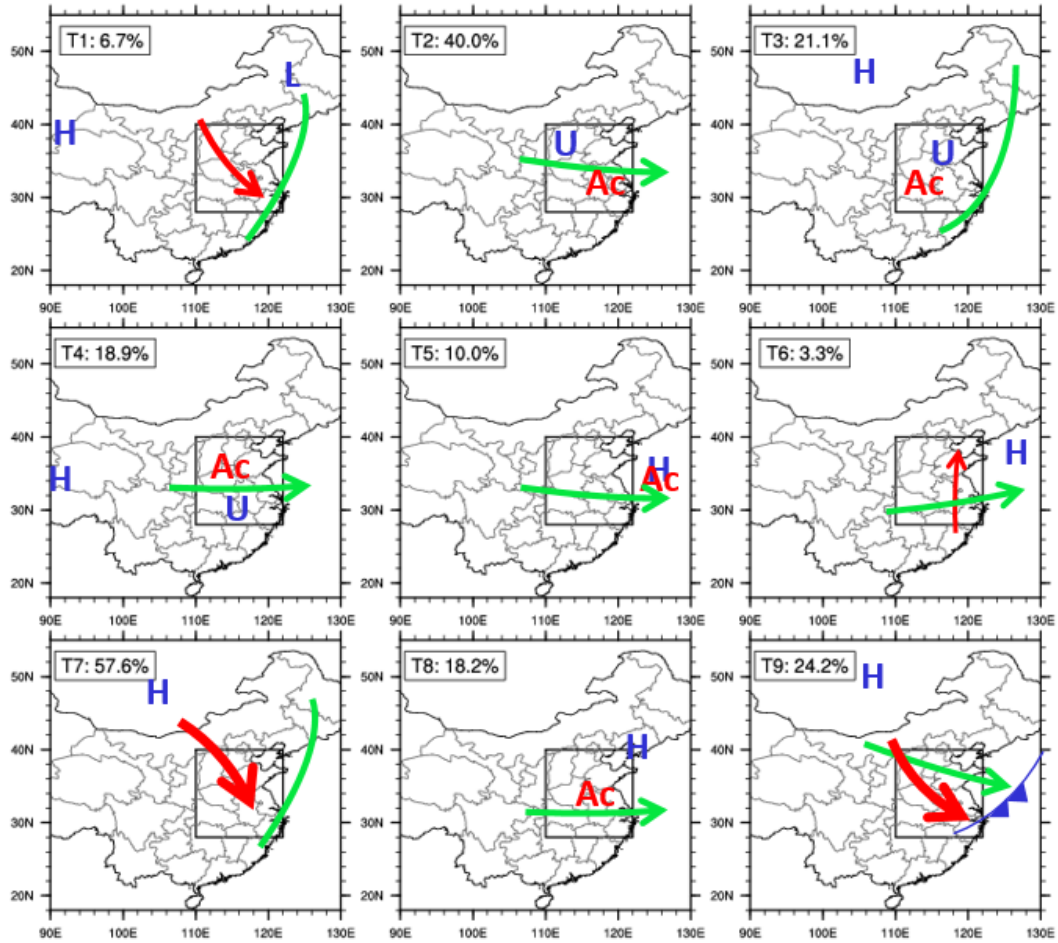


Fig.17. Schematic diagram of nine circulation types. The surface, 850hPa level and 500hPa level are shown by blue, red and green marks, respectively. At surface, “H/L” is the location of high/low pressure centers, “U” means a uniform pressure field in East China. At 850hPa, “Ac” represents for the existence of an anticyclone, and the red arrow is used to indicate the wind direction and speed. At 500hPa, the green marks are used to indicate the direction of upper air flow or the location of trough line.

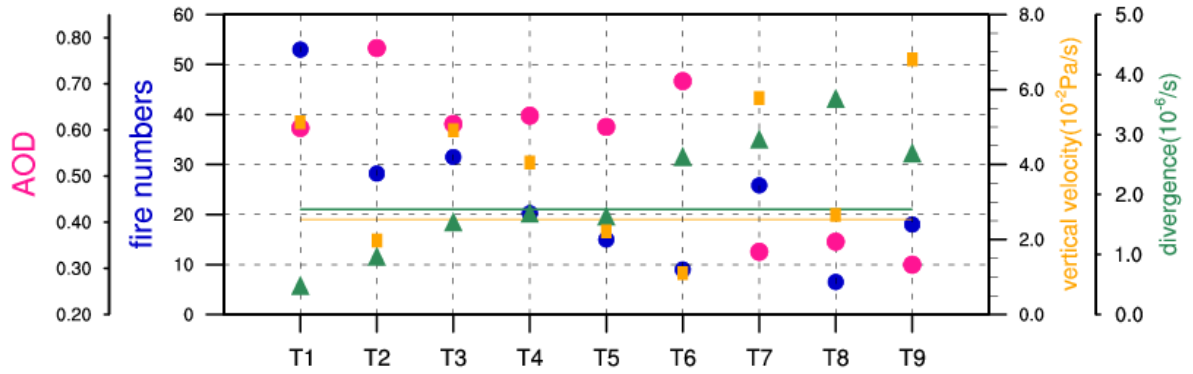


Fig.18. The values of AOD (peach), fire numbers (blue), vertical velocity (orange), and divergence of low level winds (green). The orange and green lines represent for the climatological average of vertical velocity and divergence, respectively. T1-T9, namely Type 1- Type 9, mean the nine different types summarized in this study.